Aalto-yliopisto
Aalto-universitetet
Aalto University

1

Master’s Programme in Mechanical Engineering

Data Driven Analysis of Ship Performance in various ice conditions.

Ameer Hamza Arif

Master’s thesis
2025

Aalto-yliopisto
Aalto-universitetet
Aalto University

Author: Ameer Hamza Arif	
Title of thesis: Data Driven Analysis of Ship Performance in Various Ice Conditions.	
Programme: Master's Programme in Mechanical Engineering	
Major: Mechanical Engineering	
Thesis supervisor: Assistant Professor Mashrura Musharraf	
Thesis advisor(s): Assistant Professor Mikko Suominen & Dr. Liu Cong	

Date: 24.11.2025 **Number of pages**: 65 **Language**: English

Abstract

Maritime activity in polar regions is increasing due to climate change, resulting in the opening of new Arctic Sea routes for commercial shipping. This increases the importance of reliable ship performance methods to ensure operational safety and economic viability. Classical methods such as Lindqvist and Malmberg are conservative and are developed based on simplifications. The increasing volume of actual ship machinery data and ice data provides a good opportunity to develop data-driven methods. Existing data-driven studies are based on coarse AIS datasets with limited machinery information. Additionally, they rarely provide a comparison with h-v curves developed using classical methods.

This thesis investigates data-driven methods for predicting the performance of a ship navigating in ice using machinery-aware full-scale sea trial data. It compares the data-driven methods with classical semi-empirical models by constructing h-v curves for the PSRV S.A. Agulhas II and Aranda using various machine learning techniques. Different machine learning regressors were trained on full-scale data by segregating the data based on various ice conditions (level and ridge ice).

In the case of level ice, the raw sensor logs were time-synchronized and filtered to select only level-ice data while the ship was moving straight ahead. Outliers in the (h,v) data were removed using a Mahalanobis-distance filter and a correlation-based feature selection to retain the most predictive variables. The Extra-Trees ensemble achieved the highest predictive accuracy on in-sample test data. The resulting data-driven h-v curves lie above the Lindqvist-based h-v curve, indicating its conservative nature.

In case of ridge ice due to the noncontinuous nature of loads and resistance, 30s bins were created, and a 33s delay was rectified in ice thickness and speed. Polynomial and Extra-Tree models were used for the creation of the h-v curve using the mean values of the bins. Both of these models indicated a monotonic loss of speed with increasing ridge thickness. The data-driven h-v curves and the Malmberg-based curve agree on the overall trend, but the Malmberg tends to predict higher speeds than those implied by the measured and learned curves.

To conclude, when ample high-quality data is available, machine learning regressors can be effectively used for overall performance predictions, particularly in level ice, and for averaged performance estimates in ridge ice. However, they are not well suited for instantaneous performance prediction in ridge ice conditions.

Keywords: h-v curve, ship speed, level ice, ridge ice, ship performance, data driven

Table of contents

Preface and acknowledgements

I want to thank my supervisor, Assistant Professor Mashrura Musharraf, and my thesis advisors, Assistant Professor Mikko Suominen and Dr. Liu Cong, for their good advice and guidance.
Otaniemi, 24 November 2025

Symbols and abbreviations

Symbols

h_{EM}	Ice thickness measured with electromagnetic device [m]
h	Equivalent ice thickness [m]
H_v	Equivalent-volume ice thickness [m]
H_p	Equivalent performance ice thickness [m]
v	Ship velocity
h_{keel}	Ridge keel thickness [m]
h_{SC}	Ice thickness measured with stereo camera [m]
c	Ice concentration
ρ	Porosity of unconsolidated ice rubble
μ	Friction coefficient
α_k	Base angle of ridge keel [°]
B	Breadth at waterline (m)
w_k	Ridge keel width or ridge width [m]
C_d	Ice floe size correction coefficient
d	Ice floe diameter [m]

1 Introduction

In recent years, maritime activity in polar regions has been growing rapidly, shifting from scientific exploration to significant resource extraction and commercial shipping. Reduction in sea ice coverage due to climate change is opening new Arctic Sea routes for longer periods. By the end of this century, the Northern Sea Route across the Arctic Ocean could become navigable year-round (Zhao et al., 2024). This unprecedented access to polar waters would offer shorter transit times between major markets. Therefore, it's important for ships to reliably and safely operate in harsh ice-infested waters.

1.1 Background

Understanding and prediction of ship performance in different ice conditions is of paramount importance for ship designers as well as operators. Ships navigating through ice encounter vastly different and harsh conditions as compared to open water. These can severely impact a ship's speed, fuel consumption, and structural safety. Naval architects use performance prediction models to design stronger hulls and propulsion systems for ice-going vessels. These models are also used by mariners to plan safe and efficient voyages through icy waters. With the increase in human activity in high latitudes, the need for robust performance prediction methods is increasing for economic viability and operational safety.

Different ice types impose different loads and resistances on a ship's hull. For instance, level ice involves bending of an ice sheet, whereas brash ice navigation involves overcoming friction due to granular ice mass. Therefore, a model that accurately predicts ship speed in one ice type may not directly apply to another. This indicates that each scenario should be treated separately, and combining all ice conditions into a single predictive model would introduce complexities and uncertainties.

1.2 Research motivation and objectives

Safe and efficient operation of ships in ice-covered waters requires accurate prediction of the ship's performance under various ice conditions. Traditional semi-empirical models, such as the Lindqvist method for level ice resistance, have been used in engineering practices. However, these models are known to rely on simplified assumptions and conservative calibrations. For instance, Lindqvist's method was derived from full-scale tests in the Bay of Bothnia and tends to overestimate resistance for modern hull forms (Jeong, 2013).

This conservatism (while useful for design safety) can lead to underestimation of a vessel's actual capability in moderate ice conditions, resulting in suboptimal route planning or excess powering. On the other hand, full-scale sea trials and continuous monitoring systems are generating increasing volumes of data on ship performance in ice. This opens the door for data-driven modeling techniques to learn complex ship–ice interaction patterns directly from measurements, potentially improving prediction accuracy and breadth of applicability. The motivation of this research is to leverage modern machine learning methods to improve ship performance prediction in ice while doing a comparison with existing semi-empirical approaches.

Such comparisons can reveal the strengths and limitations of each approach. For example, quantifying how much of the real performance variance an empirical formula fails to explain or determining whether a Machine Learning (ML) model might be overfit to a specific ship. This thesis addresses that research gap by comparing the classical semi-empirical method with data driven models. By doing so, we aim to assess whether a data-driven method can provide more accurate and generalizable h-v curves (speed vs ice thickness) than the conventional formula.

The primary aim of this research is to develop h-v curves using full-scale data and examine how these curves differ when obtained through empirical versus ML techniques. To fulfill this aim, the work is structured around several key objectives as given below.

1. Acquire and preprocess high-resolution, full-scale sea trials data set for steady operation in different types of ice, such as level ice, ridge ice, and ice channel.
2. Develop and train several data-driven regression models (Extra-Trees ensemble and polynomial regression) using full-scale trial data from

an ice-going vessel to predict the ship's performance across different ice conditions.

3. Evaluate the prediction accuracy of these data driven models within the range of the training data and compare their performance against the classical models, such as Lindqvist and Malmberg, by h-v curves comparison.
4. Compare, evaluate, and analyze these curves against each other. This involves evaluating prediction errors and differences in curve shapes and interpreting why the models diverge.
5. Identify the data requirements and gaps for reliable model development. Documenting the deficiencies in data and models and proposing how future data collection or model enhancements could address these gaps.

1.3 Research Scope

The scope of this thesis is focused on level ice conditions and ridge ice conditions based on two different case study vessels.

Ice Conditions: The study considers two primary ice regimes encountered during the full-scale trials: level ice and ridge ice. Both of these regimes pose different challenges for modeling. The scope explicitly excludes other ice features such as pack ice with large floes, icebergs, or severe multi-year ice, since such conditions were not present in the trial data and would require separate treatment. Thus, the findings are most applicable to first-year ice conditions common in the Baltic Sea or similar environments.

Vessel and Data: All data used for model development and validation come from full-scale trials of Polar Supply and Research Vessel (PSRV) S.A. Agulhas II and Aranda; the trained models are therefore ship specific (Suominen et al., 2020). The dataset includes measurements of ship speed, engine power, ice thickness, and other relevant variables logged during each trial run. Transient maneuvers or highly unsteady episodes (such as ramming or backing in ice) are not explicitly modeled, since the data driven approach here targets quasi-steady operating conditions. In ridged ice, which are transient by nature, average resistance or speed is considered. It includes forward motion in level ice (i.e. the ship breaking continuous ice) and in ridged ice.

Models Compared: The thesis compares data driven models vs. a theoretical empirical model. The data driven models, as noted, are (1) an Extra-Trees ensemble regressor (an ensemble of randomized decision trees) and (2) a polynomial regression model. These were selected to span a range from fully non-parametric (Extra-Trees) to fully parametric (polynomial). On the theoretical side, the Lindqvist (1989) formula for level ice and Malmberg (1983) method is used for ridge resistance.

The intent is to provide a clear and controlled comparison under well-defined conditions. So that we can draw insights about data driven modeling efficacy and its potential to complement classical approaches in similar contexts.

This thesis consists of multiple sections, and the upcoming sections are organized as follows. Chapter 2 provides a broader picture of various studies done on the topic of ship performance in ice. It also reviews various ice conditions and their effect on ship operations. Chapter 3 begins by outlining the source and nature of the data used and its preprocessing. It includes the h-v curve generation procedure by using both empirical methods and data driven models.

Chapter 4 presents the core findings of the study. It showcases the h-v curves produced by each method and examines their differences. This chapter delves into reasons behind the discrepancies, and the performance of each model is considered in terms of accuracy and practicality. Chapter 5 summarizes the contributions and key takeaways of the research as well as recommendations for future work.

2 Literature review

Ship performance in ice involves multiple factors such as ship geometry, ice resistance, and propulsion performance (Jeong, 2024). Ice resistance is defined as the force that opposes the ship movement as it navigates through ice-covered waters. Ice resistance can be decomposed into several components, including crushing, bending and submersion resistances (Lindqvist, 1989). These components are affected by ship design factors like hull angle and displacement etc. They also depend upon different environmental factors such as temperature and weather conditions which influences the mechanical properties of ice (Kaj, 2007). Upcoming sections explains different types of ice and then talks about various models and studies done for ship performance assessment.

2.1 Ice conditions

Sea ice occurs in various forms and degrees of deformation, each of which can significantly impact a ship's navigability, resistance, and structural loads. Different ice types and formations can significantly impact a vessel's navigability, resistance, and structural integrity. The World Meteorological Organization (2014) classifies sea ice by deformation state: level ice (undeformed) versus deformed ice that has been reshaped by pressure processes. Common deformed types include rafted ice and ridged ice, while navigational channels having broken ice represent another important scenario. Following section discusses each ice type its influence on ship performance.

2.1.1 Level ice

Level ice is defined as "sea ice which has not been affected by deformation," characterized by its relatively smooth, flat surface formed under calm freezing conditions (World Meteorological Organization, 2014). It represents the undisturbed initial growth phase of sea ice before mechanical forces act upon it. It can range from thin sheets (e.g. young ice) to thick first-year ice, but its defining feature is a relatively uniform, smooth surface. It provides a continuous barrier that a ship must break through by bending or crushing the ice ahead of its bow. This usually results in a steady or periodically cyclic resistance force on the hull as the ship advances and breaks the ice piece by piece. In essence, level ice presents a distributed and relatively predictable resistance load that dictates propulsion requirements. It is often the baseline case for evaluating ice going ship performance, and many empirical or analytical ice resistance formulas are formulated for level ice conditions. For example in case of empirical formulas some of the classical methods are Enkvist (1972), Lindqvist (1989) and Riska et al. (1997) while analytical methods include Norman (1980), Valanto et al. (2001) and Lubbad and Løset (2011) etc.

2.1.2 Rafted ice

Rafted ice refers to a form of deformed sea ice where "one piece of ice overriding another," typically occurring under compressive stress when thin, flexible ice floes collide (World Meteorological Organization, 2014). This process leads to layered ice structures and is an early deformation mechanism in seasonal ice zones. Rafting is most common in new or young ice when the ice sheets are thin and brittle, though it can occur in thicker first-year ice during early winter or spring thaws.

The presence of rafted ice means a ship will intermittently encounter ice that is thicker (and heavier) than the surrounding level ice. Rafted ice's structural strength can be lower than an equivalently thick single layer, because the bond between the layers may fracture easily (Huang et al., 2024). This can make rafted ice somewhat easier to break through than solid level ice of the same total thickness. However, the sudden thickness changes and layer interfaces in rafted ice lead to more concentrated loads on the ship's hull. As the ship breaks through the upper layer and then the lower layer, the resistance force tends to peak when the bow contacts the thicker overlapped sections.

2.1.3 Ridged ice

Ridged ice, or pressure ridges, are formed when sea ice undergoes strong convergence and fracturing, leading to an elongated accumulation of broken ice blocks piled haphazardly one upon another. These structures consist of a visible sail above the surface and a submerged keel below, significantly influencing the mechanical and thermodynamic behavior of the ice cover (Weeks

& Hibler, 2010). Pressure ridges are often the most formidable obstacles in sea ice navigation. Because ridges concentrate a large mass of ice into a narrow line, they can present forces well above those of the surrounding level ice. When a ship encounters a ridge, it must break a mix of ice blocks and consolidated ice in the ridge. Ridged ice demands careful navigation and in order to avoid damage ships must slow down, use ramming techniques or seek routes around the largest ridges.

2.1.4 Broken ice channel

A broken ice channel is a navigational channel through sea ice that is filled with fragmented ice pieces rather than an intact ice sheet. These broken pieces, often called brash ice, are the wreckage of other forms of ice. Such a channel is usually created by icebreaking operations (Matala & Suominen, 2022). For example, an icebreaker plows through level ice, leaving a trail of broken ice in its wake. Essentially, the channel becomes a long pile of loose or semi-consolidated ice rubble. Navigating in a brash ice or broken ice channel differs from level ice travel in that the ship is not breaking a solid sheet ahead of its bow but rather pushing through a congested mixture of ice pieces. If the channel is fresh (recently broken) and the brash ice layer is relatively thin, this scenario can be easier on the ship than intact level ice.

However, brash ice channels introduce significant resistance of their own. The ship experiences frictional and form resistance from plowing through the ice rubble (Li & Huang, 2022). The ice fragments constantly grind along the hull, especially near the waterline and along the bow and shoulders, increasing drag. From an operational standpoint, broken ice channels are both a help and a hindrance: they enable ships to travel through ice fields they could not penetrate in intact form, but the ships must be prepared for significant continuous resistance and the possibility of getting stuck if their power is insufficient.

2.2 Ship performance methods

Ship performance is evaluated through various methods such as full-scale tests, model-scale tests, analytical formulas, semi-empirical formulas, and numerical simulations. Full-scale trials provide the most realistic data on ice forces, but they are expensive and logistically challenging. Ice-tank experiments offer a more economical way to study hull-ice interactions and verify designs.

Early research from the 1970s onward used analytical formulas calibrated from test data to estimate resistance and speed. Although these methods have been invaluable for design, they generally assume simplified hull and ice geometries. Resulting in extensive simplification of ship-ice interactions and inability to predict maneuvering behavior (Li et al., 2020). A classic example is the Lindqvist formula developed in the 1980s, which estimates level-ice resistance based on hull geometry and ice properties. These formula-based methods are invaluable for design and have formed the backbone of ice engineering for decades. In the upcoming section we will briefly discuss various empirical, numerical and analytical method however data driven methods are explored in detail to understand the work done so far and what contributions can be made in that aspect.

2.2.1 Empirical formulas

Empirical formulas, such as Lindqvist (1989) and Riska et al. (1997) ice resistance model, provide practical approximations by decomposing resistance into bending, crushing, and submergence components. However, these formulas rely on simplifications calibrated to specific hull geometries and ice conditions, limiting their applicability in dynamic or non-uniform ice environments (Erceg & Ehlers, 2017). For instance, they often assume continuous level ice and steady-state motion, which means they may not capture complex phenomena like ship inertia or intermittent breaking patterns; effectively, the ship is treated as moving at constant speed through an infinite ice sheet.

2.2.2 Numerical methods

Development of numerical and hybrid analytical models has accelerated over the past few decades. Researchers have developed sophisticated simulations to model ship-ice interaction by considering material deformation, fracture, and fluid dynamics. One of the earliest numerical frameworks for level-ice manoeuvring was presented by Lindström (1990), who formulated mathematical models to estimate a ship's turning performance in level ice.

Valanto et al. (2001) extended this approach by coupling potential-flow theory with finite-element models of ice breaking and rotation and by using Lindqvist (1989) semi-empirical method to compute submergence resistance A notable later development is the Lubbad and Løset (2011) model, which derives closed-form solutions for the initial ice-breaking phase and then simulates the movement of broken ice pieces numerically (Li et al., 2020).

Beyond these representative models, a variety of simulation techniques ranging from cohesive-element methods, discrete-element methods (DEM), fluid-structure interaction (FSI), and finite-element methods have been used for ice-breaking processes. DEM models represent ice as collections of discrete particles or blocks; this approach has been used to reproduce the breaking and clearing of ice floes around a hull. For brash-ice channels, recent reviews observe that DEM has become the dominant numerical tool and that coupling computational fluid dynamics with DEM (CFD-DEM) is increasingly used to capture both ice particle interactions and hydrodynamic effects (Gong, 2023). Similarly, FEM has been applied using Abaqus to estimate the bending behavior of the floating ice sheet (Sawamura et al., 2008). Despite their power, these numerical simulations often require assumptions or simplifications to manage computational cost such as reducing dimensionality, simplifying ice failure criteria, or using empirical ice-hull friction coefficients.

2.2.3 Model-scale tests

Model-scale tests use small-scale ship models in controlled tanks (ice basins or refrigerated towing tanks) to measure ice resistance and operability. They are considered a reliable method to evaluate ship performance in ice, especially to assess channel resistance in brash ice (Xie et al., 2022). Controlled physical tests allow direct measurement of ice loads and resistance under realistic (frozen) conditions. Model tests are much cheaper and safer than full-scale trials however they involve scale-model laws and material adjustments that introduce uncertainties when extrapolating to full-scale. Because the model is small, the model ice must be made significantly weaker than real sea ice so that it breaks in a realistic way (Franz von Bock und Polach & Ehlers, 2015).

2.2.4 Data driven methods

Data driven approaches have the potential especially to cover diverse ice conditions. Unlike purely physics-based approaches, statistical or machine-learning methods learn from real voyage and environmental data that can capture complex interactions. However, the success of data-driven models depends on the quality of input data, and in ice navigation this is a major challenge. A widely used data source for Baltic studies is HELMI (Helsinki Multi-category) sea-ice model that outputs ice conditions on a 1 nautical mile × 1 hour grid (Haapala et al., 2005). Therefore, it provides spatially coarse ice data, missing fine-scale ice features around a ship giving uncertain estimates for local ice conditions. It is essentially a legacy 2D model with limited thermodynamics that has not been updated for years (Westerlund & Lehtiranta, 2025).

Machine learning and statistical regression: Numerous studies have applied ML and regression techniques to predict ship speed from environmental data. Data driven approaches have the potential especially to cover diverse ice conditions. ML methods such as neural networks, support vector regression, decision trees, and ensemble models have proven effective at capturing complex, nonlinear interactions between vessel speed, power, and other machinary and environmental variables (Gan et al., 2025).

In case of ice navigation, Milaković et al. (2020) simulates ship speed in complex ice using ANN. Its also uses the data from full-scale ice tests of PSRV S.A. Agulhas II given by Suominen et al. (2013). However this study doesn't analyse the ship speed in comparison to available theoretical or empirical methods such as Lindqvist (1989) and Malmberg (1983).

Similarly, there are other studies that leverage large-scale AIS (Automatic Identification System) logs, ice charts, and remote sensing for speed prediction without the need of full-scale tests. For example, Similä and Lensu (2018) developed a regression model using features extracted from syntheticaperture radar (SAR) ice images, together with AIS ship data, to estimate the speed of independent ice-going vessels in the Baltic Sea. They trained a Random Forest regressor on matched AIS tracks and ice-thickness, finding that about 65–82% of predicted speeds, normalized per ship, were within 1–1.5 speed units of the true speeds. One of major limitations in their work was the absence of machinery data such as power and pitch of the propellers. Zhang et al. (2022) demonstrated successful ANN based h-v curve generation for inland waterways while comparing with other models. Their study focuses on operational scheduling based on aggregated model test data from multiple ships. However, it only assumes level ice, doesn't perform any filtering and doesn't include pitch of the properller as a feature.

In the Arctic context, Rao et al. (2021) demonstrated that gradient-boosted decision-tree models (XGBoost, LightGBM, etc.) trained on AIS tracks and spatiotemporal features (time of year, location, daylight, etc.) can predict vessel speed even without explicit ice input. Using tanker voyages in the Barents and Kara Seas (2017–2019), they achieved mean absolute errors around 3.5 knots on unseen test data. This result highlights that rich AIS-based features can capture implicit ice effects through location/time, though larger errors in choke points (Kara Strait) suggest missing ice-state information.

Across these studies, random forests and gradient boosting have frequently emerged as top performers for ship speed prediction. LightGBM and XGBoost often outperform simpler methods, likely because they effectively handle mixed categorical and continuous inputs and limit overfitting (Gan et al., 2025; Rao et al., 2021).

Hybrid and ensemble models: In general, ensemble strategies, e.g., combining multiple ML algorithms or blending with first-principles outputs, have shown promise in recent ship-performance studies, but their use in ice navigation is still emerging. Montewka et al. (2019) combined a semi-empirical model for ridged ice at near 100% concentration with a data-driven model for mixed conditions and the icebreaker effect. They merged AIS logs and ice-chart data for an IA Super bulk carrier and found that the hybrid approach could predict realistic speeds across a wide range of conditions.

Bayesian and probabilistic models: Probabilistic methods, especially Bayesian models, are effective in quantifying uncertainty in ship-ice interactions. Montewka et al. (2015) pioneered the use of Bayesian networks (BNs) to model ship speed and besetting risk in dynamic ice conditions. The study demonstrated BNs' capability to capture the joint effects of ice variables and adapt predictions with new data for operational route optimization but faced limitations due to low-resolution ice forecasts and neglect of crew decision impacts on speed.

Building on this, Fu et al. (2016) developed a besetting risk model for Arctic waters using data from the Yong Sheng voyage. Their Bayesian Belief Network (BBN) integrated environmental and ship parameters, validated through sensitivity analysis, identifying ice concentration and wind speed as key risk factors. Li et al. (2017) extended this line by building a BN with full-scale data to yield a probability distribution over discrete speed categories given the ice conditions. Such BN models explicitly incorporate uncertainty and feature dependence, which can be valuable for risk-aware navigation. However, challenges remain in generalizing these models across various ship classes, regions, and ice types, with prospects in merging real-time forecasts with machine learning for enhanced adaptive route planning.

Physics-informed ML techniques: While classical ML models treat the speed–ice relationship as a black box, recent work is exploring ways to integrate physical knowledge and improve uncertainty estimation. One direction is physics-informed machine learning. For example, Lang et al. (2024) proposed a physics-informed model combining a neural-network surrogate for calm water speed with a gradient-boosted model for ice effects. In their approach, a Physics Informed Neural Network (PINN) is trained to reproduce a known speed–power curve (from model test data) under calm water conditions, while an XGBoost model learns the speed reduction in ice from AIS data. By coupling the two in parallel, the model respects known ship dynamics yet corrects for ice-induced losses. This hybrid PINN+XGBoost scheme yielded more physically consistent and accurate predictions than a pure data-driven model.

2.3 Ice thickness vs ship speed curve

The ice thickness (h) vs ship speed (v) The H-V curve is a performance-defining metric for continuous navigation in ice and is the most fundamental measure for assessing the performance of ice-going ships (Izumiyama, 2017). It charts maximum attainable continuous speed for a specific ice thickness. It reveals a strong negative correlation between ice thickness and attainable speed. Traditionally, it has been used employing semi-empirical approaches to estimate ship performance in ice. The curve can be developed by analytically modelling the ship's attainable speed (v) as a function of level ice thickness (h). The methodology is based on establishing a condition of equilibrium where the required ice resistance is balanced by the propeller net thrust (Su et al., 2010). The h–v curve stands as a fundamental metric for quantifying continuous operational capability. It is highly significant because it relies on physical principles and explicitly outlines the ship's continuous performance envelope.

2.4 Literature review findings

From the synthesis of literature, it becomes apparent that certain research gaps and opportunities exist. Many of the data driven studies to date have relied on coarse AIS-based data with limited variables. There is novelty in combining a machinery-aware full-scale dataset (i.e., the one including engine power and propeller pitch, etc.) with different regressors for predictive modeling. As Similä and Lensu (2018) noted, lack of power setting information in AIS is one of the fundamental limitations. By using datasets that do contain this information (e.g., synchronized power and ice measurements from trials) and applying ML, we can produce models that inherently account for how crews and machinery react to ice (not just the ice itself). Another gap involves the derivation of h-v curves from full-scale data using machine learning regressors and their systematic comparison with curves generated by classical empirical and semi-empirical formulations. This thesis addresses these gaps by deriving ship-specific h-v curves from machinery-aware full-scale data, assessing their strengths, weaknesses, and domains of validity, and comparing them against established models.

3 Methodology

This chapter includes step-by-step methodology from data filteration to h-v curve generation using both data driven and empirical models.

3.1 Data aquisation and processing

This chapter first discusses the data sources for both ship operations and ice conditions. It then presents the raw datasets and highlights the principal challenges associated with them.

3.1.1 Ship data

The S.A. Agulhas II is a Polar Class 5 icebreaking research and supply vessel. The ship gains its power from a diesel-electric propulsion system of four diesel generators, each producing 3 MW. Two 4.5 MW electric motors provide power for two controllable pitch propellers. Table 1 lists important parameters and dimensions of this ship taken from "S. A. Agulhas II" (2025) and Suominen et al. (2013).

Table 1 Dimensions of PSRV S.A. Agulhas II. Adapted from Li (2016).

Symbol	Value	Unit	Description
B	21.7	m	Beam of the ship
T	7.65	m	Draft of the ship
L	121.8	m	Length
ϕ	27	degrees (°)	Flare angle at bow
ψ	42	degrees (°)	Hull normal angle at bow
α	33	degrees (°)	Waterline opening angle
D_p	4.5	m	Propeller diameter
v	14	knots	Service speed
Δ	13687	t	Displacement
I_z	1.77×10^{10}	kgm^5	Mass moment of inertia about the z-axis

3.1.2 Level ice data

Full-scale sea trial data used in this study is obtained from the tests described and attached as supplementary material in Suominen et al. (2020). It includes three types of tests: straight ahead in level ice, breaking out from the ice channel, and turning in level ice. Table 2 gives an overview of full-scale sea trials used in this study. PS and SB denote port and starboard sides, respectively. According to Suominen et al. (2020), visual observation in the selection of the test location was done to have level ice for L1-L3.

Table 2 Summery of full-scale ice trials conducted in different ice conditions. Adapted from Suominen et al. (2020).

Test ID	Run	Ice Condition	Start time UTC	End time UTC
L1	Ahead	Level ice field	21.3. 6:59:00	21.3. 7:05:00
L2_1 and L2_2	Ahead	Level ice field	21.3. 10:13:00	21.3. 10:41:00
L3	Ahead	Level ice field	21.3. 14:12:30	21.3. 14:22:30

Two independent instruments were used to measure sea-ice thickness: a stereo-camera system (SC) mounted at the bow shoulder and an electromagnetic induction sensor (EM) located near the forward perpendicular. Throughout, we denote EM derived thickness by h_EM and SC derived ice thickness by h_SC. Figure 1 compiles time-series from three test legs (L1-L3). In each plot, h_EM is plotted in blue and h_SC in orange against elapsed time (minutes).

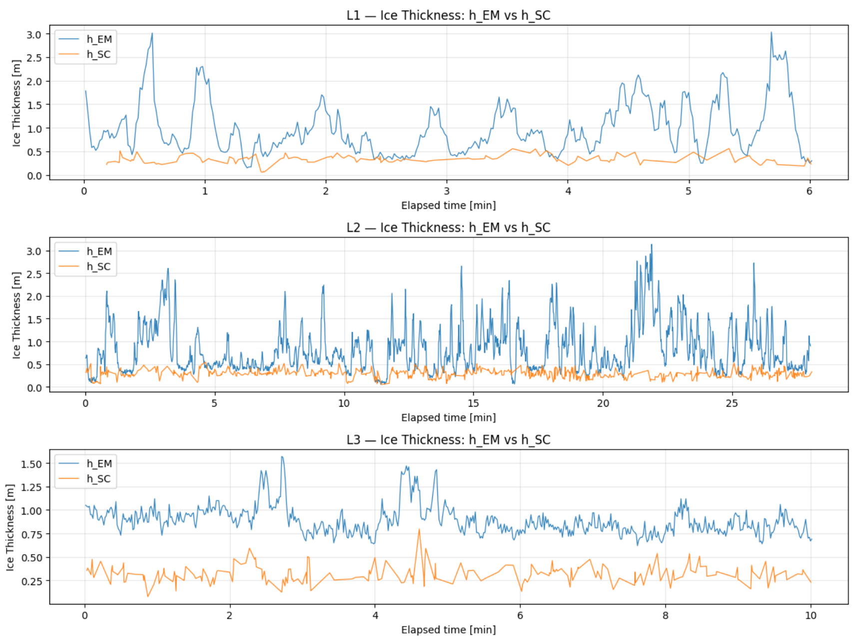

Figure 1 EM and SC ice thickness for level ice (L1, L2, L3).

L1, L2, and L3 journeys were selected for analysis, as the ship is moving straight ahead in level ice during these journeys. Continuous level ice conditions are quite rare in natural sea ice, and there are some ridges as reported by observers. To tighten the selection, a comparison was done between the instantaneous ice thickness (h_{EM}) measured by the hull-mounted electromagnetic sensor (EM) and the ice thickness measured by the stereo camera (h_{SC}). In level-ice conditions the two independent techniques are expected to agree closely; however, the EM method tends to read larger values when loose ridge blocks extend below the consolidated sheet or when rafting is present (Suominen et al., 2020). Consequently, only those data points were retained that satisfied $h_{EM} \leq 1.5\, h_{SC}$, i.e., the EM value did not exceed the stereo-camera estimate by more than 50%. This tolerance allows small rubble pieces yet effectively removes periods dominated by ridging or rafting (Li et al., 2017). For all subsequent analyses, h_{SC} is used as the primary thickness variable because the stereo-camera technique has been shown to provide the most reliable estimate in level-ice conditions (Li et al., 2018). Stereo camera data is more reliable in predicting level ice thickness and in medium and low power usage regions it's around 0.3 meters.

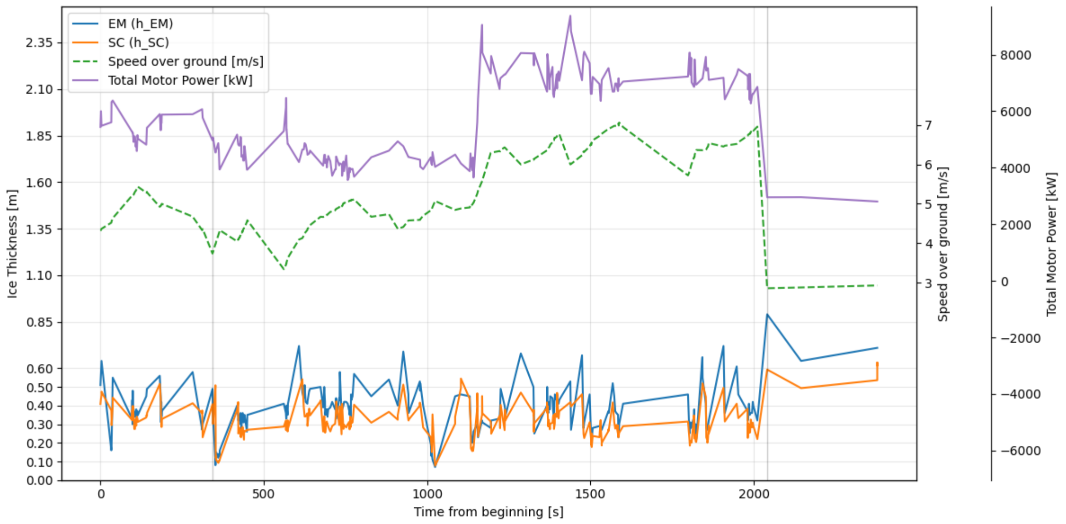

Figure 2 Ice thickness, speed over ground, and total motor power plot in case of level ice.

Figure 2 summarizes the level-ice run. The left axis shows ice thickness, the right axes show speed over ground and total motor power. Thickness remains in the moderately thin range. Initially there is a lower speed/power region followed by a mid run step up in speed with a proportional increase in power.

3.1.3 Ridge ice data

In case of ridge ice the data is taken from the full-scale tests of the Aranda (SYKE & FMI, 2016) as attached in the supplement of Li et al. (2018). Ice thickness was measure using EM31 device. To obtain periods of ridge ice criteria given by Li et al. (2018) was followed. According to this criterion only those periods of data was selected as ridge ice where h_{EM} is less than 3 m and ship speed fluctuates.

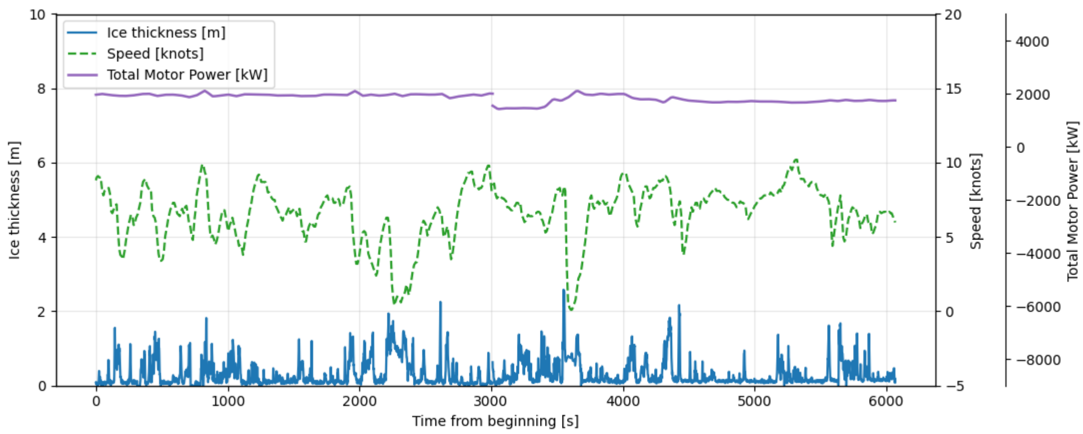

Figure 3 Variation of speed w.r.t power and ice thickness for the two runs of Aranda in ridged ice

Figure 3 presents a long run with ice thickness, speed and total motor power. The ship is operated at an almost constant power setpoint, while v fluctuates as the encountered thickness varies. The thickness spikes are primarily absorbed by speed reductions rather than large power surges.

A key feature of the record is that the response is not instantaneous. The troughs in the speed lag the peaks in ice thickness and speed recovery after thin patches is similarly delayed. This lag arises from ship inertia and propulsion control dynamics. Therefore, point-by-point pairs would not provide the actual effect of change in one variable over the other.

3.1.4 Ice properties

Since the full-scale trials of PSRV S.A. Agulhas II were performed within 2x2 km, ice properties are assumed to be uniform across this area. Ice's flexural strength was tested to be 404 kPa, which is typical for Baltic spring ice (Suominen et al., 2013). Table 3 lists some of the important properties of ice.

Table 3 Ice properties in Baltic Sea. Adapted from Suominen et al. (2013).

Symbol	Parameter	Value
σ_b	Flexural strength of ice	404 kPa
E	Elastic modulus	1.0 GPa
ν	Poisson ratio	0.3
ρ_w	Density of water	1025 kg m^{-3}
μ	Friction coefficient	0.15
ρ_i	Density of ice	900 kg m^{-3}

3.2 Data-driven analysis of level ice

In this section different methods and techniques are discussed and applied to the filtered level ice data to preprocess the data for effective implementation of data-driven methods. Then, based on the range of data and correlations between different features and our requirements, two suitable ML methods are described.

3.2.1 Data synchronisation

Full-scale trials data of PSRV S.A. Agulhas II described in Section 3.1.2 produced multi-sensor time series from independent onboard systems: two ice-thickness channels (EM and SC), navigation (ship speed, course, heading) and propulsion/machinery (port/starboard motor power, propeller pitch, shaft RPM, rudder angles). Each subsystem is logged by a separate data source with its own sampling rate and latency. Synchronization is essential because performance models (e.g., v–h–P) require that ice thickness, speed and machinery state all refer to the same physical instant. A naïve row by row merge of the raw logs would mix measurements taken at different times. Hence smearing cause–effect relationships that will bias regression coefficients towards zero.

To ensure a consistent analysis of the multisensor data, all datasets were aligned using a nearest neighbor matching approach based on the universal time coordinate (UTC_Time). The SC ice thickness series was used as the

reference timeline because thickness is treated as the exogenous driver of resistance and performance. For every SC timestamp, the corresponding speed, heading, power, pitch, RPM, and rudder angles are taken from the nearest available observation in each respective stream, subject to a small maximum time difference. This one-sided nearest-neighbor matching in time effectively down-samples the higher-frequency sensors to the ice-thickness rate while keeping the temporal error below one sampling interval.
Nearest in time matching to a reference sensor is a common and practical choice in multi-sensor fusion when sampling rates differ, as shown, for example, in inertial vision navigation filters where camera images are aligned to the closest IMU sample (Caruso et al., 2017). Each merged output provides a comprehensive, time-resolved view of ship-ice interactions, enabling consistent evaluation of cause-effect relationships between hull dynamics, propulsion, and ice load events.

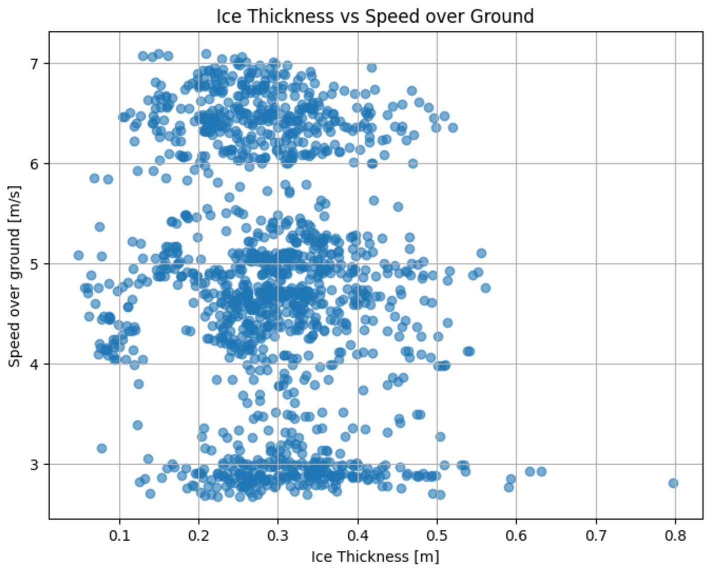

Figure 4 Scatter plot presents observed speed and ice thickness data.

Figure 4 shows a scatter plot of speed against ice thickness. The data points form three clusters that likely correspond to trial runs conducted at full, medium, and low propulsion levels. The first cluster centres around 3 m/s (5.8 knots) while the second and third centres around 4.5-5 m/s and 6.5-7 m/s respectively. Most data points lie within a narrow band of ice thicknesses (0.2–0.4 m).

3.2.2 Outlier removal and boundary points

To flag physically implausible combinations of ice thickness (h) and ship speed (v) without imposing axis-aligned cut-offs, a bivariate Mahalanobis-distance filter was applied. First, the two-dimensional vector x = [h, V] was extracted for every 1 Hz record (N observations). The empirical mean μ and covariance Σ of this cloud define the expected elliptical scatter under the assumption of approximately Gaussian measurement noise. Mahalanobis distance is suitable here because it accounts for the different scales and correlation between h and v, providing a rotationally invariant measure of how typical each pair (h,v) is. For each observation i, the squared Mahalanobis distance

$$D_i^2 = (\mathbf{x}_i - \boldsymbol{\mu})^\top \Sigma^{-1} (\mathbf{x}_i - \boldsymbol{\mu}) \qquad (1)$$

quantifies how far it lies from the centroid when correlations between (h) and (v) are taken into account. Because D^2 follows a χ^2 distribution with p = 2 degrees of freedom, points beyond the 97.5% quantile were deemed multivariate outliers, yielding a cleaned dataset that retains the statistically coherent central 97.5% ellipse of the (h,v) distribution. The scatter plot in Figure 5 visually confirms that the procedure trims only a handful of peripheral points (black = purple, yellow = red) while preserving the main data structure.

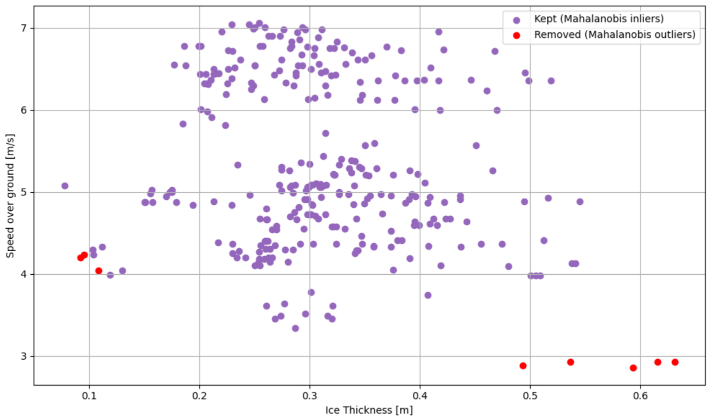

Figure 5 Mahalanobis Outlier Dectection: Speed vs Ice Thickness Plot.

The histogram of the ice thickness [m] observations in Figure 6 shows that more than half of all measurements fall between 0.25 m and 0.35 m, confirming that data collection was concentrated in medium ice. Values below

0.15 m and above 0.45 m occur only sporadically; the histogram tails are very thin. In particular there are virtually no points below 0.05 m (open water) and only a handful above 0.50 m. This imbalance means that any regression surface fitted directly to the raw data will be well constrained around 0.3 m but potentially unreliable at the low and high ends of the operating envelope. As shown in Figure 13, h-v curve generated using Lindqvist method ranges from 0 (open water) to 1.25 at high power.

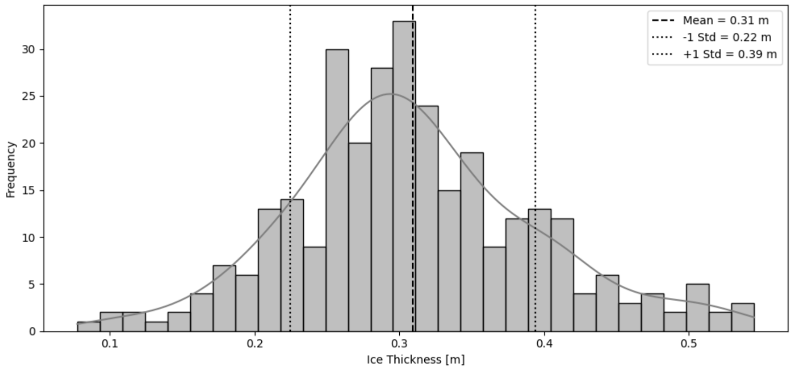

Figure 6 Distribution of ice thickness with mean and spread.

Relying purely on the full scale would force the model to extrapolate beyond its empirical support, a common source of large prediction error. To cater to this problem, open water speed can be included in the training set (14 kn at 0 m ice) at maximum power operation ("S. A. Agulhas II", 2025; Suominen et al., 2013).

3.2.3 Feature selection

The outlier-screened dataset was pruned of features that are not related to ship performance. The temporal identifier (UTC_Time) was only important for synchronisation and was therefore discarded, while geographic coordinates were removed because the objective is to relate vessel speed to changes in ice properties and machinery settings. As discussed in Section 3.3.1, ice thickness from the stereo camera was to be used for the analysis; hence, electromagnetic ice thickness was excluded.

Exploratory visual analysis: Before applying quantitative feature selection criteria, scatter plots were created for ship speed against other features. The plots show that propeller pitch and motor power are the dominant controls on speed. Power vs speed plots in Figure 7 show distinct clusters and as the ship opearates at higher power setting speed is also higher. The ice thickness vs speed plot also shows clusters due to different power settings. Since the ice thickness range is very narrow therefore its difficult to see a clear trend however for both the clusters as it moves towards higher thickness the speed seems to drop. Heading separates the data into a few angular clusters corresponding to different track directions, but within each cluster speed varies widely with no obvious monotonic trend.

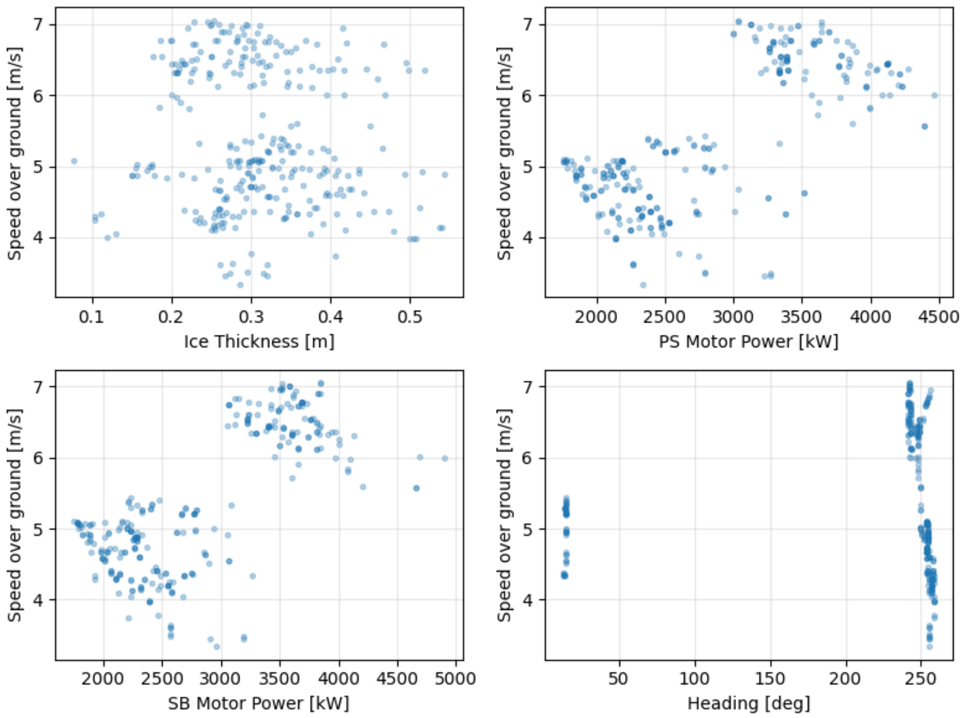

Figure 7 Scatter plots of ship vs (a) ice thickness, (b) PS motor power, (c) SB motor power, and (d) ship heading.

Both rudder position plots in Figure 8 show a dense vertical band near 0° and 1°-2° rudder angle. Even though large manoeuvres are absent in this dataset small systematic offset between the runs is visible. This corresponds to slightly different resistance faced. Both PS and SB propeller pitch plots in Figure 8 show tight, upward sloping clouds of points, with higher pitch percentages corresponding to higher speeds and trend is close to linear. The scatter plots for shaft RPM as given in Figure 9 is clustered around 140 and shows different speed level mainly due to change in power rather than acting as an independent control variable. It suggests that RPM carries little unique information for predicting speed once power and pitch are included.

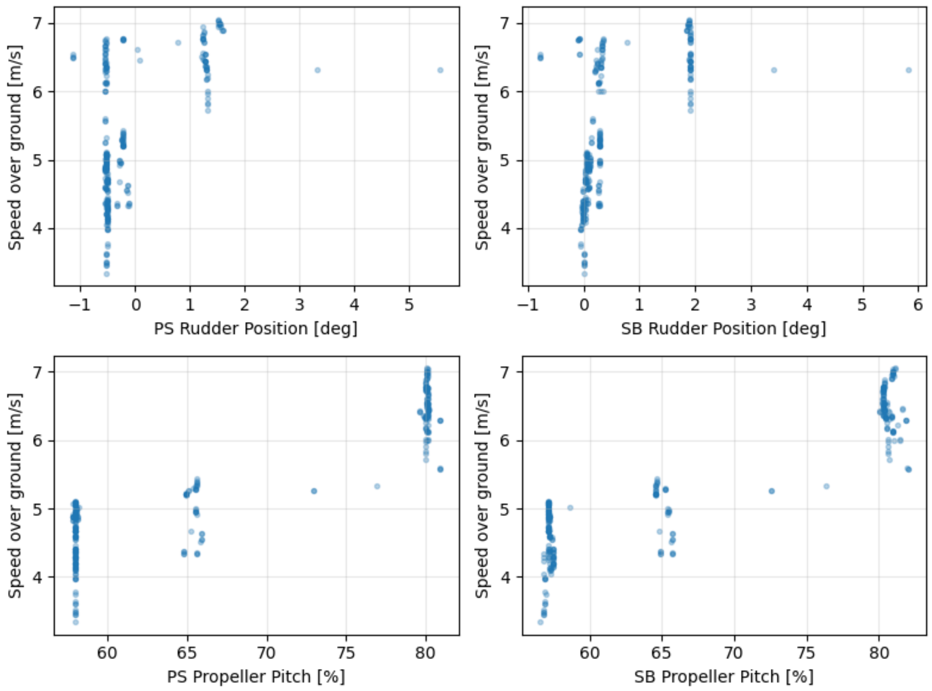

Figure 8 Scatter plots of ship speed vs (a) PS rudder position, (b) SB rudder position, (c) PS propeller pitch, and (d) SB propeller pitch.

Overall, the exploratory plots indicate that (i) propeller pitch and motor power have strong, almost linear relationships with speed; (ii) ice thickness shows only a modest influence within the sampled range; and (iii) RPM and heading show no useful direct structure.

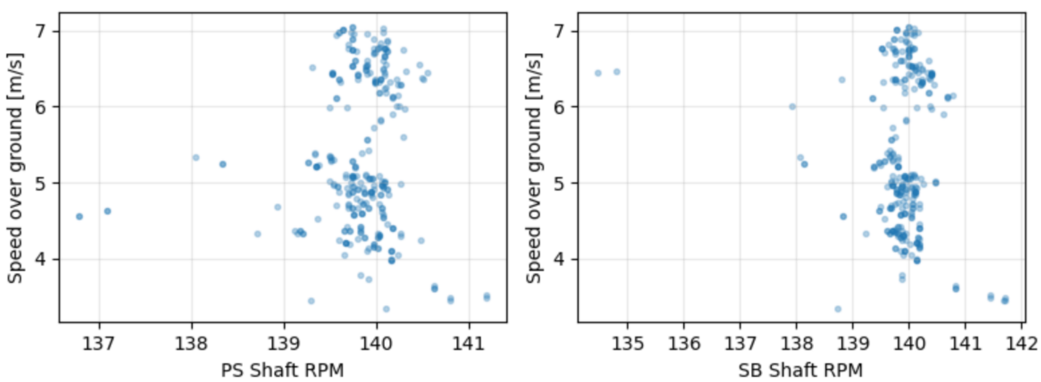

Figure 9 Scatter plots of speed vs (a) PS shaft RPM and (b) SB shaft RPM.

Pearson and Spearman Correlations: A simple filter-based feature selection method based on Pearson's product-moment correlation was employed to identify variables most strongly associated with the response variable, ship speed. Pearson correlation quantifies the strength and direction of linear relationships between pairs of variables and is calculated as the covariance between two variables divided by the product of their standard deviations as given in Equation 2. Since it is inherently scale-invariant, no standardisation of the variables was necessary. For two continuous variables X and Y, Pearson's correlation coefficient r is defined as

$$r_{XY} = \frac{\mathrm{cov}(X,Y)}{\sigma_X \sigma_Y} = \frac{\sum_{i=1}^{n} (x_i - \bar{x})(y_i - \bar{y})}{\sqrt{\sum_{i=1}^{n} (x_i - \bar{x})^2}\sqrt{\sum_{i=1}^{n} (y_i - \bar{y})^2}} \tag{2}$$

where are $\bar{x}$, $\bar{y}$ are sample means and σ_X, σ_Y are the sample standard deviations. The coefficient r_{XY} takes values in [-1,1]: |r|= 1 indicates a strong linear relationship, whereas r = 0 suggests little or no linear dependence.
To also detect monotonic but potentially non-linear relationships, Spearman's rank correlation ρ was evaluated. Spearman's ρ is simply the Pearson correlation computed on the ranked values of the variables. If R_X and R_Y denote the ranks of X and Y, then

$$\rho_{XY} = r_{R_X R_Y} \tag{3}$$

In the special case without ties, this reduces to the well-known formula.

$$\rho_{XY} = 1 - \frac{6\sum_{i=1}^{n} d_i^2}{n(n^2-1)} \tag{4}$$

where d_i is the difference between the ranks of x_i and y_i.
Because Spearman's ρ is based on ranks, it measures how well an arbitrary monotonic function (not necessarily linear) can describe the relationship between X and Y. A predictor can therefore have a small Pearson r but a relatively large Spearman ρ if the association is curved yet monotone. Both of these coefficients were computed for each numeric predictor against the speed using the outlier-filtered level-ice dataset. The resulting Pearson and Spearman correlations are given in Table 4.

Table 4 Correlation of ship speed to features.

Variables [Unit]	Pearson's r	Spearman's ρ
PS Propeller Pitch [%]	0.913	0.831
SB Propeller Pitch [%]	0.912	0.753
SB Motor Power [kW]	0.738	0.640
PS Motor Power [kW]	0.716	0.626
SB Rudder Position [deg]	0.599	0.700
PS Rudder Position [deg]	0.558	0.239
Ice Thickness [m]	-0.112	-0.114
Heading [deg]	0.105	-0.607
Course over ground [deg]	0.102	-0.620
SB Shaft RPM	-0.102	-0.007
PS Shaft RPM	0.052	-0.009

Propeller pitch (PS and SB) shows the strongest positive linear association with speed, with $r = 0.91$ and $\rho = 0.83$ and 0.75, respectively. This confirms the visual impression from the scatter plots: higher pitch settings correspond almost linearly to higher speeds over most of the operating range.

Motor powers also exhibit a similarly strong positive relationship, with r around 0.72 and ρ around 0.63. Increasing delivered shaft power thus clearly increases attainable speed.

The rudder positions' correlation with speed ($|r| = 0.56–0.60$, ρ up to 0.70) indicates a significant effect on speed. Ice thickness has only a weak negative correlation with both r and ρ equal to -0.11. Within the narrow level-ice range of roughly 0.25–0.50 m, variations in h are therefore largely masked by the crew's power and pitch adjustments. Therefore, the ice thickness does not emerge as a strong statistical driver in this subset, despite its fundamental physical importance. Heading and course over ground have very small Pearson correlations with speed ($|r| = 0.10$), indicating almost no linear effect. Spearman's ρ is moderately negative; however, as shown in scatter plots, this arises from a few discrete heading bands associated with different runs rather than from a genuine monotonic dependence. Shaft RPM (PS and SB) exhibits negligible correlation with speed ($|r| \leq 0.10$ and ρ close to zero), consistent with RPM being largely determined by the commanded power and pitch. Once those primary control variables are included, RPM adds little independent information.

In a nutshell, the correlation analysis confirms that propeller pitch and motor power are the dominant predictors of speed, with ice thickness exhibiting only a modest effect in the available level ice data.

Predictor-predictor correlations: After ranking predictors against speed, a second correlation analysis was performed to assess redundancy and potential multicollinearity between predictors. For this purpose, a Pearson correlation matrix was computed for all candidate features, as shown in Figure 10.

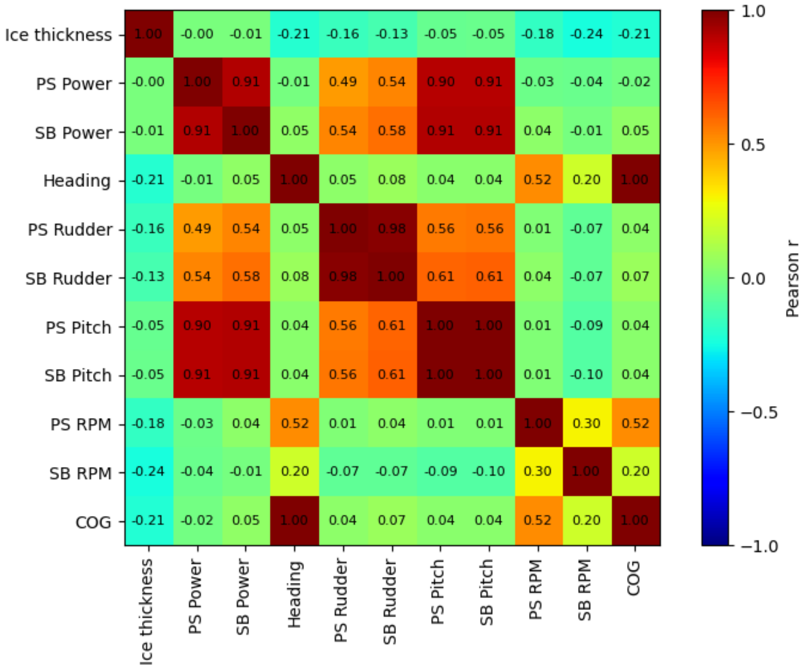

Figure 10 Predictor- predictor Pearson correlation matrix for all the features in case of level ice.

PS and SB propeller pitch, motor power, and rudder positions are strongly correlated. The correlation matrix shows that the main source of redundancy arises from the symmetry of port and starboard measurements. Therefore, these pairs should be replaced by physically meaningful combined quantities (e.g., total motor power and mean rudder position) rather than keeping separate PS and SB channels. Similarly, propeller pitch and motor power are also strongly correlated.

Reduced feature set and rationale: The exploratory plots and correlation analyses indicate that both propeller pitch and shaft power are strongly associated with ship speed. In contrast, variables such as heading, course over ground, and shaft RPM show no meaningful relationship with speed and were therefore excluded from further modelling. From a data-driven perspective, features with very high correlation ($|r| = 0.9$) are considered redundant. Since propeller pitch and power are highly collinear and both reflect propulsion level, keeping both would add little new information while increasing redundancy. To reduce dimensionality and avoid multicollinearity, only power was retained. Power is also more straightforward to control and interpret in practical settings.

PS and SB powers are themselves highly correlated. These were therefore combined into a single feature: total motor power, computed as the sum of the PS and SB shaft powers. This transformation preserves the total propulsion level while eliminating duplicate information from symmetric sensors. The same symmetry argument applies to rudder angles: PS and SB rudder positions are strongly correlated, but both represent the same steering command. They were therefore merged into a single descriptor, the mean rudder position, which captures the effective straight-ahead steering state while avoiding duplicate channels.

Ice thickness measured by the stereo camera was retained as the main environmental variable. Although it shows only a weak correlation with speed, it is not strongly correlated with any machinery variable and therefore provides independent information about external conditions. The final reduced feature set used in the subsequent regression therefore consists of three non-redundant and interpretable predictors: ice thickness, total motor power, and mean rudder position. This set focuses on the key controllable machinery and steering parameters, while variables that are either weakly related to speed or strongly collinear with these predictors are excluded.

3.2.4 Data-driven methods for level ice

When the training set is dense in one region and thin in another, the choice of regression family has a pronounced impact on predictive reliability. A low-order polynomial is a global parametric surface: every coefficient is estimated from every sample, so the fitted curve must pass smoothly through the entire range of the predictor, even where data points are scarce. In practical terms, the quadratic model borrows strength from the rich 0.25-0.35 m band to stabilize its predictions for extrapolation. In contrast, tree-based models such as Random Forests and Extra Trees generate predictions that are piecewise constant. Each unseen test point is forced into the terminal leaf whose boundaries happen to enclose it; if that leaf is populated by only one or two training samples, the prediction inherits their noise unfiltered. Hence, stepwise methods risk flat spots, sudden jumps, or spurious peaks precisely where the data provide the least guidance.

Polynomial regression: Although no purely data-driven model can guarantee accuracy outside the observed domain, a quadratic polynomial behaves in a physically intuitive way: the response grows (or decays) at most quadratically with the predictor. Second-order (quadratic) polynomial regression extends multiple linear regression by including squared terms and pairwise interactions of the predictors, allowing the model to capture moderate curvature in the response. For n input variables $x_1, \ldots, x_n$ the model can be written as:

$$y = \beta_0 + \sum_{i=1}^{n} \beta_i x_i + \sum_{i=1}^{n} \beta_{ii} x_i^2 + \sum_{i=1}^{n-1} \sum_{j=i+1}^{n} \beta_{ij} x_i x_j + \varepsilon, \tag{5}$$

where y is the predicted output, β_0 is the intercept, β_i are the coefficients for the linear (main) effects of each x_i, β_{ii} are the coefficients for the quadratic terms x_i^2, β_{ij} are the coefficients for the interaction terms $x_i x_j$, and ε represents the residual error.

Extra trees regressor: The Extra Trees regressor is an ensemble algorithm that builds many decision trees for regression. Each tree is constructed by recursively splitting the training data (using the entire dataset, no bootstrap sampling) until termination. In this context, a node refers to any point in the tree that partitions data, and a leaf (terminal node) is a final subset of data where no further splitting occurs. The final prediction of the ensemble is obtained by averaging the outputs of all the individual trees. Because the trees are randomized, this averaging tends to produce a stable, low-variance predictor (Geurts et al., 2006).

A single regression tree has a hierarchical structure of internal (split) nodes and leaf nodes. The top of the tree is the root node, representing the full dataset. At each internal node, the data is divided by testing one feature against a threshold value, which splits the data into two child branches. These branches lead to further internal nodes or eventually to leaf nodes. A leaf node corresponds to a final region of the input space: all inputs reaching that leaf yield the same constant prediction. In a regression tree, the prediction at a leaf is typically the mean of the target values of the training samples in that leaf. Equivalently, one can write a tree's prediction as

$$\hat{f}(x) = \sum_{m=1}^{M} c_m \mathbf{1}\{x \in R_m\} \tag{6}$$

where R_m are the leaf regions and c_m is the average target in R_m.

Extra trees differ from ordinary trees in how each split is chosen. At each internal node, the algorithm selects a random subset of features, and for each selected feature, it picks a split threshold uniformly at random from that feature's range. Each of these random candidate splits is scored (for example, by how much it reduces variance), and the best one is used to divide the data. In this way, cut points are not optimized by exhaustive search but are instead randomly drawn. By default, Extra Trees grow each tree on the entire training set (no bootstrap sampling), so all trees see all data. This extreme randomization (in both feature choice and threshold value) tends to decorrelate the trees and reduce variance across the ensemble.

After all trees are built, a new input x is run down each tree until it reaches a leaf, and each tree outputs that leaf's stored value (the mean target for the training points in the leaf). The Extra Trees regressor's final prediction is the average of these tree outputs. Formally, if $h_t(x)$ is the prediction from tree t and there are T trees, the ensemble prediction is

$$\hat{y}(\mathbf{x}) = \frac{1}{T}\sum_{t=1}^{T} h_t(\mathbf{x}) \tag{7}$$

Each $h_t(x)$ equals the constant value cmc_mcm of the leaf region R_m that contains x. Averaging these values yields the final regression estimate. In summary, the Extra Trees regressor builds a forest of highly randomized trees (with random feature and threshold selection at each node) and makes predictions by averaging the trees' outputs.

3.3 Data driven analysis of ridge ice

In the case of ridges, the resistance and hence the speed don't remain constant. When a ship encounters a ridge, it moves through it based on its inertia and loses its kinetic energy in the process. Therefore, the ship doesn't reach its minimal speed at the very moment the sensors report higher ice thickness. To cater to the transient nature of loads and the complex profile of ridged ice, this section discusses time correction and segmentation of the ice legs for meaningful implementation of data driven methods. So instead of modeling a single ridge and predicting the speed across it, the key focus is on the average speed against average ice thickness for a leg of ice.

Therefore, it's not predicting the instantaneous speed at the specific points of a single ridge. It acts as a filter that removes high-frequency inertial noise, aligning this method with the theoretical equilibrium model developed using Malmberg and available thrust.

3.3.1 Time delay and segamentation

As observed in Figure 3 and discussed in Section 3.1.3 there is a delay in input ice thickness and ouput ship speed. Estimating this input to output delay is very important to avoid smearing of cause-effect relationship by using simultaneous samples. Additionally, to obtain steady state, segmentation should be done to create ice legs or bins and then compute the median ice thickness for each bin. These time synced bin averaged h,v pairs will effectively smooth the transient lag. The hull load, propellers and engine system have inertia and control-loop dynamics, so shaft speed and delivered power respond over seconds to tens of seconds to load changes. Typically, transient load variations are 5–15 s or longer, confirming a physical delay between resistance changes and achieved speed (Acanfora et al., 2022).

Lagged cross-correlation is used to estimate the transport delay between ice thickness and ship speed. Causal lags were scanned and the correlation between h(t) and v(t+L) was computed. The lag L with maximized |corr| was chosen. Speed responds 33 samples later to thickness changes. With 1 Hz data, that would mean 33 s. Shifting thickness forward by 33 samples (i.e., pairing v(t) with h(t−33)) enforces causal pairing: the thickness that physically caused the observed speed is used in the pair (h,v). This reduces simultaneity bias and yields more meaningful regression curves. To obtain interpretable input-output structure from noisy and instantaneous measurements, 30 s average measurements were taken by binning the data. Binning reduces high-frequency fluctuations and measurement jitter that do not reflect quasi-steady ice-hull interaction, mitigates serial dependence, and aligns the effective temporal resolution with the system's response time (propulsor and control-loop inertia). Choosing the bin width to be on the order of the identified delay/settling horizon ensures that each aggregated point approximates a locally steady operating condition.

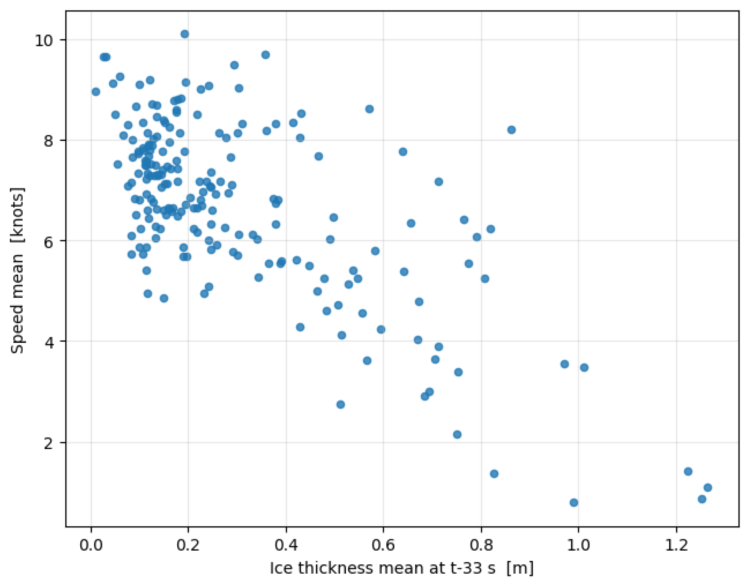

Figure 11 Ship speed vs lagged ice thickness scatter plot in ridged ice.

The scatter shows a clear inverse relationship: as lagged ice thickness increases from ~0 to ~1.2 m, the bin-level speed declines from ~9–10 kn to ~1–2 kn, consistent with higher resistance in thicker ridged ice. Variability is greatest at low thickness (<0.3 m), and dispersion narrows as thickness grows.

3.3.2 Feature selection

The correlation analysis was performed using both the Pearson correlation coefficient r and the Spearman rank correlation coefficient ρ in order to assess both linear and monotonic relationships between ship speed and the selected predictors.

Table 5 reports the absolute correlation strengths. Ice thickness shows a strong negative influence on ship speed, with |r|=0.68 and |ρ|=0.508, confirming that speed reduction is strongly associated with increasing ridge thickness. Meanwhile, motor power demonstrates only a weak correlation with speed (|r|=0.233, |ρ|=0.151), likely due to very small changes in the power across the dataset.

Table 5 Correlation of ship speed to features for ridged ice.

Variables [Unit]	**Pearson's *r***	**Spearman's *ρ***
Ice Thickness [m]	0.688	0.508
Motor Power [kW]	0.233	0.151

3.3.3 Data driven methods for ridge ice

After the lag correction and binning the scatter plot between the ice thickness and speed, most of the points lie in the cluster around 0.1-0.2 m ice thickness. Unlike level ice thickness, the dataset has observations till 1.2 m ice thickness. However, very few points exist after 0.3 m, and their density decreases as we go beyond that. In such a scenario extrapolation is needed in addition to interpolation; however, this extrapolation can be more reliable. Therefore, in the case of ridge ice, the same two models presented in Section 3.2.4, i.e., 2^{nd} degree polynomial and extra tree regression, are used. Polynomial regression provides us with smooth extrapolated curve while extra tree provides best performance and reliability for in-range data while capturing non-linearities.

3.4 Empirical methods

This section introduces the semi-empirical methods used to generate h-v curves. First, for the level ice, the Lindqvist method is described in detail. The resulting h-v curves will be compared with the h-v curve for level ice obtained from data driven models. Next, for the ridge ice, the Malmberg method is presented, and its procedure for constructing h-v curves is described. It will be compared against the ridge ice h-v curve obtained using data driven models.

3.4.1 Lindqvist method for level ice

The total level-ice resistance per unit breadth (R_{ice}) is expressed as the sum of breaking (R_b), crushing (R_c), and submersion (R_s) terms, augmented by empirical velocity corrections (Lindqvist, 1989).

$$R_{\text{ice}} = (R_c + R_b)\left(1 + 1.4\frac{V}{\sqrt{gh}}\right) + R_s\left(1 + 9.4\frac{V}{\sqrt{gL}}\right) \tag{8}$$

The terms R_c and R_b represent the resistance due to ice crushing and bending failure, respectively, while R_s accounts for the submersion of broken ice pieces beneath the hull. The velocity correction terms $\left(1 + 1.4\frac{V}{\sqrt{gh}}\right)$ and $\left(1 + 9.4\frac{V}{\sqrt{gL}}\right)$ adjust the static resistances to account for dynamic effects during ship motion.

$$R_c = 0.5\sigma_b h_i \frac{\tan\phi + \mu\cos\phi/\cos\psi}{1 - \mu\sin\phi/\cos\psi} \tag{9}$$

R_c models the resistance generated as ice is crushed by the hull. It is influenced by the ice thickness h, compressive strength σ_b, friction coefficient μ, and hull-ice contact angles ϕ and ψ.

$$R_b = \frac{27}{64}\sigma_b B \frac{h_i^{1.5}}{\sqrt{\frac{E}{12(1-v^2)g\rho_w}}} \frac{\tan\psi + \mu\cos\phi}{\cos\psi\sin\alpha}\left(1 + \frac{1}{\cos\psi}\right) \tag{10}$$

The breaking resistance quantifies the force needed to initiate and propagate flexural failure in the ice sheet. It depends on the flexural strength σ_b, breadth

B, ice thickness h_i, Poisson's ratio ν, and water density ρ_w. The geometric parameters α and ψ are determined from hull geometry and interaction with the ice.

$$R_s = (\rho_w - \rho_i) g h B \left(T \frac{B+T}{B+2T} + k \right) \tag{11}$$

This component captures the resistance arising from the need to submerge ice floes beneath the vessel's hull. It is influenced by the relative densities of water and ice, as well as the ship's draft T, beam B, and an empirical correction term k.

$$k = \mu \left(0.7L - \frac{T}{\tan \phi} - \frac{B}{4 \tan\ \alpha} + T \cos\ \phi \cos\ \psi \sqrt{\frac{1}{\sin \phi^2} + \frac{1}{\tan \alpha^2}} \right) \tag{12}$$

The term k adjusts the submersion resistance to account for hull shape and ice interaction, incorporating vessel length L, draft T, and ice-hull friction μ.

$$\psi = \arctan \left(\frac{\tan \phi}{\sin \alpha} \right) \tag{13}$$

The angle ψ represents the inclination of the wedge formed during ice interaction and is determined by the flare angle ϕ and the waterline entrance angle α.

To evaluate a vessel's operational capability in ice-covered waters, it is critical to determine the maximum attainable speed at different ice thicknesses under varying power inputs. It involves combining the Lindqvist ice resistance model with the propeller thrust model to compute the vessel's achievable speed in level ice as a function of ice thickness for different power levels.

$$R_{\text{ice}}\,(v, h) = T_{\text{net}}\,(v, P) \tag{14}$$

R_{ice} is the total ice resistance (from Lindqvist's model) and T_{net} is the available net thrust after accounting for open water losses. The net propeller thrust is estimated using empirical models for bollard pull and the admiralty coefficient given in Equation 14 and Equation 16 respectively.

$$T_B = K_E (P \cdot D)^{2/3} \tag{15}$$

Equation 15 relates installed power and propeller diameter to the thrust potential. For controllable-pitch propellers the quality factor K_E is 0.98 for twin propellers (Juva & Riska, 2002).

$$T_{\text{net}} = T_B \left(1 - \frac{1}{3}\frac{v}{v_{\text{ow}}} - \frac{2}{3}\left(\frac{v}{v_{\text{ow}}}\right)^2\right) \tag{16}$$

$$v_P = v_{\text{full}} \left(\frac{P}{P_{\text{full}}}\right)^{1/3} \tag{17}$$

Bollard pull T_B is the maximum thrust produced at zero forward speed in open water [kN], v is the relative forward velocity between the ship and the ice [m/s], and v_{ow} is the open water speed of the ship at a given power [m/s] (Li, 2016).

3.4.2 Malmberg's method for ridged ice

The ridge keel rubble is treated as a cohesionless continuum, and the resistance is decomposed into bow resistance while the hull wedges the keel rubble aside and midship resistance while rubble is pushed along the parallel body. Total ridge resistance is the sum of these components.

$$R_t = R_b + R_m \tag{18}$$

Here R_b is bow (keel-displacement) resistance and is given in Equation 19.

$$R_{\text{bow}} = C_p T h_i(x)(0.5B + h_i(x)\tan\,\psi\cos\,\alpha)(\mu\cos\,\alpha + \sin\,\psi\sin\,\alpha) \tag{19}$$

While the midship (parallel body) resistance R_m is given by Equation 20.

$$R_m = C_m T \int_{L_m} \left(h_i(x) + \left(\frac{h_i(x)}{T} - 0.5\right)B\right)dx \tag{20}$$

R_t represents the ridge-induced component at creeping speed. All the terms used in these formulas and their values for the Aranda case are given in Table 6. These dimensions and parameters of the ship are taken from (SYKE) and estimated based on the drawings and parameters given in Kuuliala et al. (2017) and Li et al. (2018).

Table 6 Terms used in the resistance formula

Symbol	Name (units)	Value
B	Breadth at waterline (m)	13.8
T	Draught (m)	5.0
L_m	Length of parallel midship (m)	33
α	Waterline half-angle at bow	30°
ϕ	Stem angle at waterline	22°
ψ	Normal angle to horizontal at bow	42°
h_i (x)	Local ridge thickness at bow (m)	0-2 m
C_p	Bow resistance coefficient (kg m^{-2} s^{-2})	7500 kg m^{-2} s^{-2}
C_m	Midship resistance coefficient (kg m^{-2} s^{-2})	45.9 kg m^{-2} s^{-2}
μ	Ship-ice friction coefficient	0.15
p	Ridge rubble porosity	0.3
φ_r	Internal friction angle of rubble (°)	52.5°
q_D	Density difference $\rho_{sw}-\rho_i$ (kg m^{-3})	126 kgm^{-3}
v	Poisson's ratio of ridge rubble	0.26
g	Gravitational acceleration (m s^{-2})	9.81 ms^{-2}

Usually in an actual rigid case, the ship operates using its kinetic energy, and the thrust is not always equal to the ice resistance. Since the ice resistance itself is not continuous and the ship does not have a quasi-steady state. However, in our study we are using the average ice thickness of an ice leg instead of using the pointwise thickness of a ridge. For an average ice thickness, the resistance would be average as well across an ice leg; therefore, the ship needs equivalent thrust to continuously operate in these conditions. Hence, using the same approach as in level ice, the propeller's available net thrust is used to calculate the speed of the ship at a given resistance and ice thickness. This is done by balancing the propulsion and ice resistance.

$$T_{net} = T_B\left(1 - \frac{v}{3v_{ow}} - \frac{2}{3}\left(\frac{v}{v_{ow}}\right)^2\right) \tag{21}$$

The bollard thrust is evaluated from the delivered shaft power P_d and propeller diameter D_p using Equation 22. Aranda is single CPP on a single shaft so K_e = 0.78 and propeller Ø = 2.60 m (SYKE) (Kuuliala et al., 2017).

$$T_b = K_e \left(P_d D_p\right)^{2/3} \tag{22}$$

The open water speed of Aranda is 13.5 knots at maximum power usage. Equation 23 is used to calculate the open water speed at 1836 kW, which is 11.64 knots.

$$v_P = v_{\text{full}} \left(\frac{P}{P_{\text{full}}}\right)^{1/3} \tag{23}$$

4 Results and Discussion

This section compares the results obtained using various models along with different simplifications and underlying assumptions. Various recommendations are given for future work about the dynamic regression models and quality of data and how it can be improved for a meaningful implementation of data driven methods. Table 7 gives a summary of the cross-validated results of the candidate algorithms for the respective ice type. Root mean square error (RMSE) in knots and R^2 of the predicted speed with respect to the original dataset are given.

Table 7 Cross-validated results for all candidate algorithms

Ice Type	Approach	RMSE	R^2
Level Ice	Polynomial Regression	0.76	0.82
Level Ice	Extra Trees Regression	0.5505	0.9214
Ridge Ice	Polynomial Regression	0.9914	0.7891
Ridge Ice	Extra Trees Regression	0.2415	0.9863

4.1 Level ice

4.1.1 Lindqvist method

Based on the data given in Table 1 and Table 3 and using equations given in Section 3.4.1, total ice resistance is calculated at various velocities and ice thicknesses as given by Figure 12.

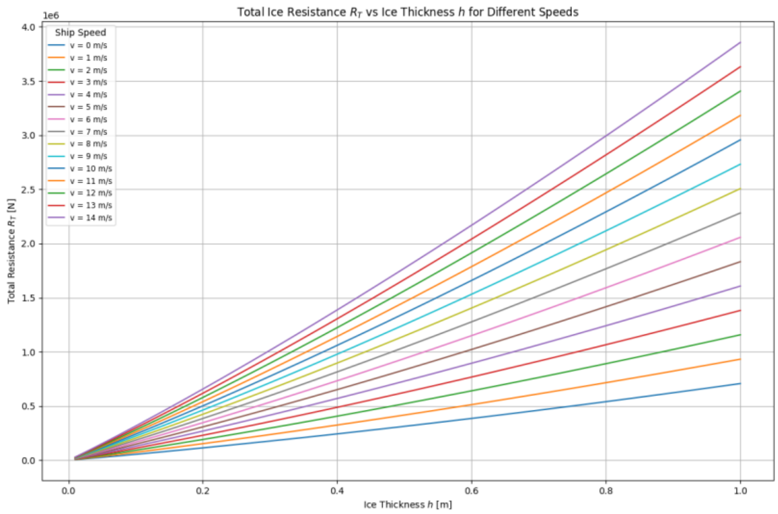

Figure 12 Ice resistance vs ice thickness using Lindqvist method.

Figure 12 illustrates the variation of total level-ice resistance R_T with respect to ice thickness h for multiple constant ship speeds, as derived using the Lindqvist empirical method. Across all curves, the relationship between total ice resistance and ice thickness is approximately linear. This is consistent with the governing equations, particularly the bending resistance Rb and crushing resistance Rc, which scale with $h^{1.5}$ and h respectively. For thin ice regimes (up to ~1.0 m), these non-linear components behave quasi-linearly, especially under relatively modest speed increases. Figure 13 presents the achievable ship speed as a function of level ice thickness, computed at average power of the dataset, i.e., 5056 kW. The ship's net thrust was calculated using the bollard pull formulation and open water correction factor, while resistance was computed using the Lindqvist method accounting for ice breaking, crushing, and submersion effects with empirical velocity adjustments.

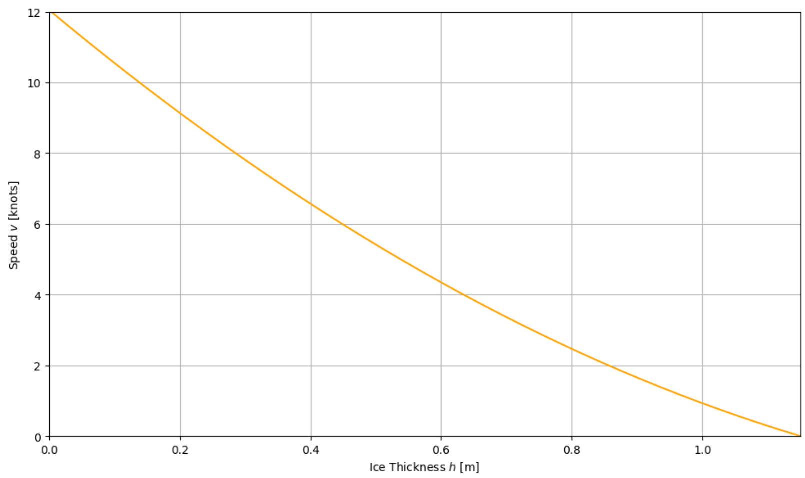

Figure 13 Ice thickness h and ship speed v curve for average power of 5056 kW developed using Lindqvist and net thrust

4.1.2 Data driven methods

A rigorous machine-learning pipeline was adopted to ensure unbiased performance estimates. The target variable, ship speed, was converted from meters per second to knots to match nautical convention. The full dataset was randomly divided into a training set (90%) and an external validation set (10%). The validation subset was withheld until the very end and used only once, providing an estimate of how the final model will behave on unseen data. The 90% training portion was further subdivided into k = 5 equally sized folds. For each of the five iterations, four folds were used to fit the model and the remaining fold to test it. Averaging the five test-fold results delivers a low-variance estimate of in-sample generalization error while still allowing every observation to contribute to training. Bootstrap sampling and randomized splits confer resilience to noise and spurious correlations.

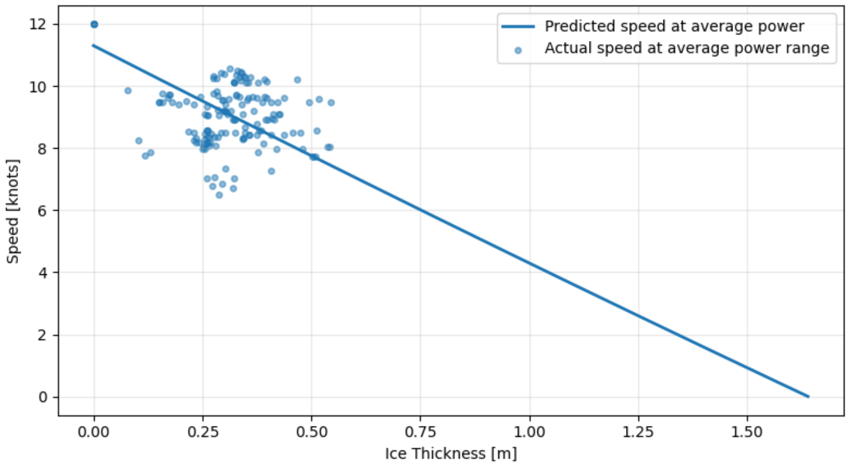

Figure 14 2nd Degree polynomial regression: Predicted speed vs ice thickness at 5650 kW.

Cross-validated RMSE for the 2nd degree polynomial is 0.76 knots, and R^2 is 0.82. Figure 14 presents 2nd degree polynomial regression surface evaluated along a single varying predictor ice thickness, while total motor power and rudder angle are fixed at the mean values of the training set.

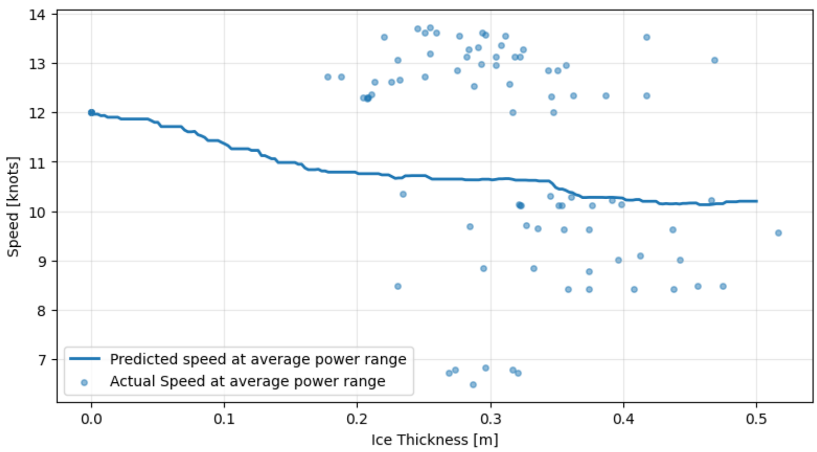

Figure 15 Extra trees regressor: Predicted speed vs ice thickness at 5650 kW.

Figure 15 shows curve fitted by extra trees regressor that provides lowest in-range error with RMSE = 0.14 kn and R^2 = 0.99. The model reproduces the expected monotone decay in speed but does so through a succession of plateaus.

4.1.3 Classical vs data-driven methods

Figure 16 shows comparison of different h-v curves obtained through Polynomial Regression, Extra Trees and Lindqvist approach. While data driven techniques are in proximity the Lindqvist curve is quite conservative. The 2nd degree polynomial provides good approximation however extra trees have minimum error while predicting within the data range confirming the presence of complex interactions among predictors. The field trial data were dominated by moderate level ice. Over half of the ice-thickness observations fell between about 0.25 and 0.35 m, with essentially no continuous ice data in open water (<0.05 m) and very few points above 0.45–0.50 m. This implies that regression models are well constrained around mid-range thickness but must extrapolate at the extremes.

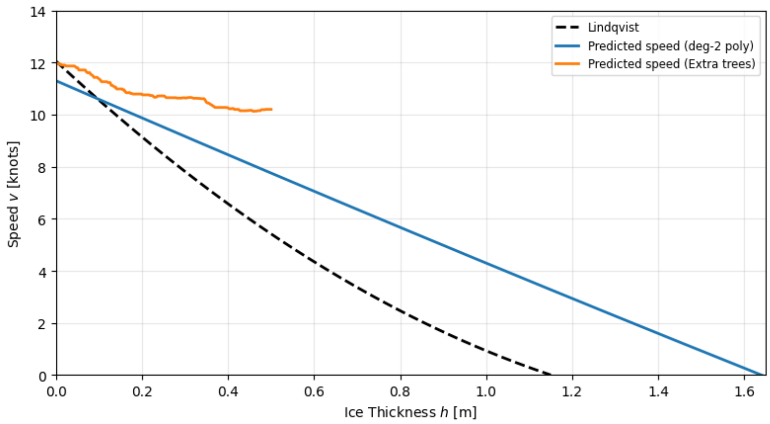

Figure 16 Speed vs ice thickness at 5650 kW - comparison of h-v curves generated using Lindqvist, Polynomial Regression and Extra Trees.

Extra-Trees are driven by local evidence, while the polynomial and Lindqvist curves impose an all-of-domain shape from the outset. That split shows up as soon as the curves move away from the bulk of observations. Extra-Trees plateaus, while the polynomial curve keeps diving according to a predefined pattern. With no data points, Extra-Trees gets stuck in the last pattern they learned while the quadratic pursues its inevitable downward trend, and Lindqvist pushes hardest because the formulas show a rapid increase in resistance with thickness. The Lindqvist curve lies well below the others, indicating much lower predicted speeds for the same ice. This conservatism arises because Lindqvist's semi-empirical formula includes all possible ice-load mechanisms (crushing, bending, etc.) in the resistance. Those mechanisms increase nonlinearly with ice thickness (roughly $\propto h^2$), so the Lindqvist equation presumes the ship will slow far more aggressively than trial observations. In practical terms, Lindqvist was derived for uniformly hard, worst-case ice, and it ignores speed-dependent effects like accumulated momentum or variable propeller pitch. Thus, its curve acts as a safety-first bound on performance in ice, i.e., a worst-case estimate.

On the other hand, the data-driven curves are learned directly from the measurements. The Extra-Trees ensemble fits every local fluctuation and drops stepwise. Overall, it predicts significantly higher speeds as compared to the other two curves given in Figure 16. Which means that Linqvist is the conservative of all. It also means that polynomial extrapolation can also be reliably used out the data range since its already a bit conservative than the actual performance. However, the downward trend for the polynomial stays linear while in reality as well as indicated by Lindvist its not linear. Therefore, beyond 1 m the prediction of polynomial is not reliable. Thus, if plenty of data range is available Extra-Trees model is highly accurate in-range (lowest RMSE) but overfits to noise and cannot extrapolate. For extrapolation polynomial can be used but should be avoided well beyond the data range. Lindqvist, meanwhile, is the most conservative and least flexible.

4.2 Ridge Ice

4.2.1 Malmberg method

Since kinetic energy change over a long window tends to zero, the mean velocity becomes a direct function of the mean energy consumption. This transforms the data from an instantaneous state to sustained performance.

While effective for generating quasi-steady-state data points for regression, this binning reduces high-frequency information regarding the ship's inertia and the impulse response of the hull colliding with ice blocks. It flattens the dynamic peaks and troughs, effectively modeling the average ship speed rather than the instantaneous ship speed. Based on this simplification and using the total resistance along with the thrust as given in Section 3.4.2 the speed is predicted at 1835.6 kW power.

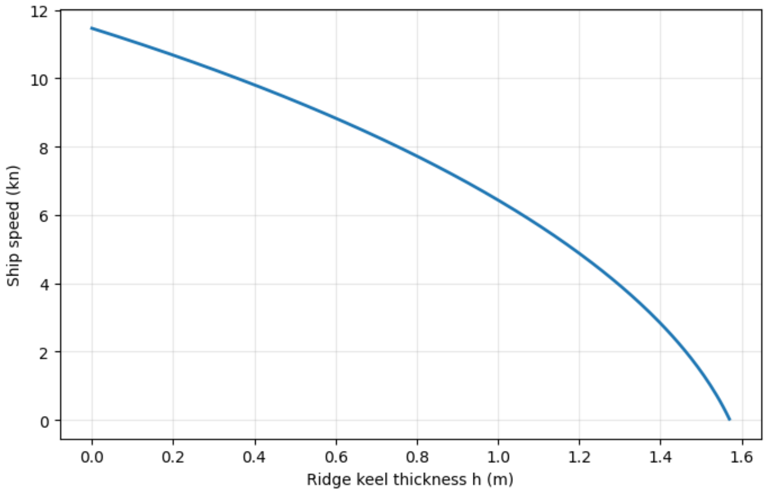

Figure 17 Ice thickness and ship speed in ridged ice, developed using Malmberg and net thrust at 1835.6 kW.

Figure 17 shows increase in resistance with increase in ice thickness and the resistance rises faster than the available net thrust, producing the smooth, monotonic decline in speed.

4.2.2 Data-driven methods

Applying the 33 s input-output delay from the lag scan and aggregating into 30 s bins clarifies the causal relation between ridge thickness and attainable speed. Figure 20 indicates thickness is the primary monotone driver since the power have minimal variations during the trial run. The delay-alignment and binning suppress simultaneity bias and short-term control transients. Two predictive models were trained on the causally aligned, binned data with power fixed at the dataset mean 1835.6 kW.

Polynomial regression: The quadratic model provides a low-variance baseline that captures smooth curvature. In the Figure 18 scatter points are mean values of 30s bins, the solid line is the quadratic model's prediction of ship speed as a function of ice thickness, evaluated at mean delivered power. The model attains $R^2 = 0.712$ and RMSE = 1.171 kn with 3-fold CV. A quadratic polynomial regression offers a low-variance, parametric baseline that captures curvature and a first-order interaction between thickness and power while remaining easy to interpret and extrapolate.

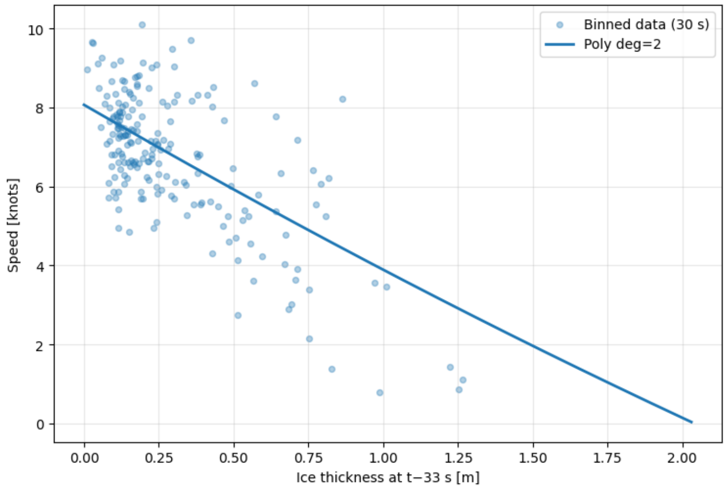

Figure 18 2nd Order polynomial fitted between mean speed and ice thickness with power fixed at 1835.6 kW.

Extra trees regressor: The Extra-Trees model yields slightly better generalization within the data range and reproduces local plateaus. Figure 19 shows the prediction of ship speed evaluated at mean power of 1835.6 kW. The model attains $R^2_{test} = 0.73$ and RMSE = 1.134 kn with 3-fold CV.

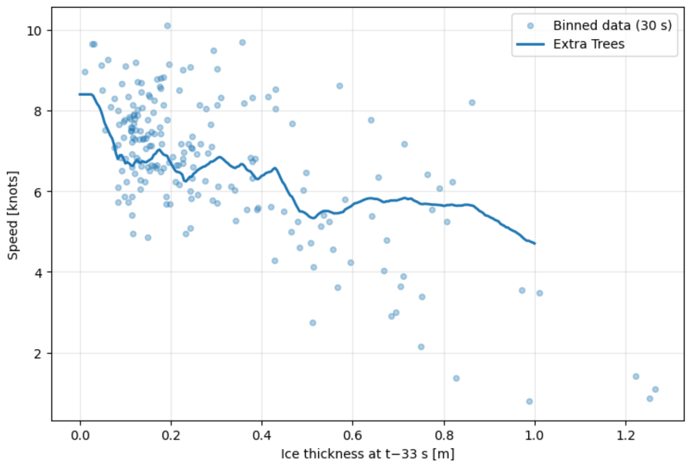

Figure 19 Extra-Trees regression curve with power fixed at 1835.6 kW.

Evaluated at the mean power, both predict a decreasing attainable speed with increasing thickness; the tree model generalizes slightly better within the data range, while the polynomial offers coefficient-level interpretability and can be extrapolated to maximum operable ice thickness at this power level.

4.2.3 Classical vs data-driven methods

Data-driven models and the Malmberg-thrust balance agree on the trend and on the order of magnitude of operability limits. Extrapolation beyond the observed thickness range (1.2 m) is unreliable with the polynomial. The Malmberg curve is anchored to the open-water reference (11.6 kn at 1836 kW), which is missing in the data driven methods.

Additionally, the h-v curve obtained using the Malmberg method shows higher speed as compared to the data driven methods primarily due to less ice resistance in the case of Malmberg. It does not incorporate the level ice and consolidated layer resistance as well as any resistance due to snow. Since the ice thickness is averaged out for an ice leg, there is no straightforward way to have consolidated layer ice thickness, which can be obtained if the thickness of different parts of the ridge, such as the keel and sail, etc., are available. However, the data driven approach is using the average of total ice thickness for an ice leg, resulting in an average resistance being faced by the ship.

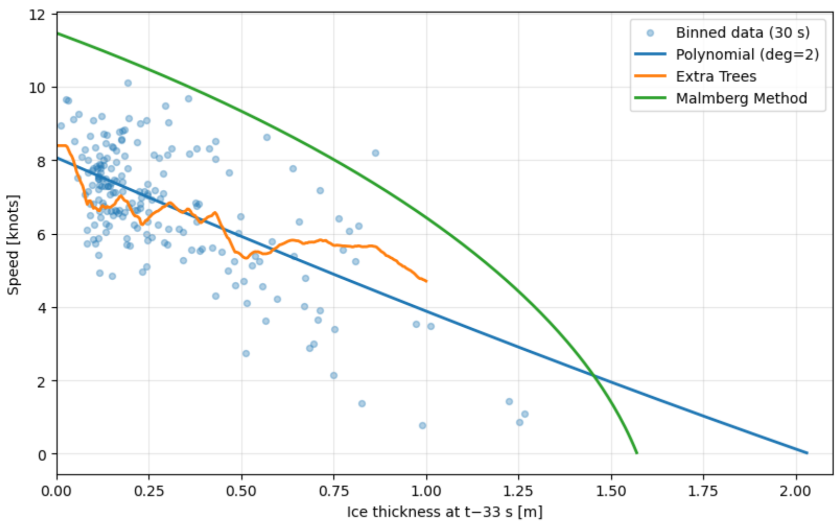

Figure 20 Speed vs ice thickness at 1836 kW - comparison of h-v curves generated using Malmberg, Polynomial Regression and Extra Trees.

The success of data-driven methods depends on data availability and quality. Additional samples are needed at both ends of the h–v range. Open-water points are easy to obtain; high-thickness points are operationally challenging due to besetting risk, especially in heavy ridging. Purpose-designed steady-state trials with calibrated ice-state variables will most effectively reduce uncertainty and enable robust model comparison.

At very small thicknesses (<0.2–0.3 m), the measured speed is usually lower, sometimes due to the start of the journey, while in the case of Malmberg combined with the available thrust method, it's set to the highest achievable value. Similarly, applying the Malmberg method on averaged-out ice thickness results in smooth resistance instead of actual variable loads due to ridging.

In reality, even traversing thin ridges involves turbulence, rubble acceleration, and hydrodynamic interaction that a static model ignores. The data-driven model, trained on real-world energy consumption, inherently captures these effects. As the ridges are not modeled but rather averaged out. So, the findings of the study can be used for an average estimate for voyage planning, but they cannot be used for the estimation of besetting risk. By utilizing time-binning and lag correction, the transient dynamics of ridge penetration are integrated into an effective velocity metric.

5 Conclusion

In level ice, the Extra-Trees regressor provided the closest match to trial data and successfully captured local nonlinear trends. The polynomial regression model was slightly less accurate but remained interpretable and could be cautiously extrapolated beyond the training range. The Lindqvist curve consistently produced lower speed predictions, confirming its conservative nature and value as a safety-oriented baseline.

In ridged ice, time-alignment and 30-second binning were required for a meaningful analysis. The Extra-Trees model again produced strong in-range predictions, while the polynomial curve offered smooth behavior where measurements were sparse. The empirical Malmberg curve predicted higher speeds at very thin ridges, as it assumed immediate access to open-water performance, which was not always achieved in measurements.

Overall, the study shows that machine-learning models can enhance ship performance prediction when high-quality data are available. Classical empirical methods remain important when extrapolation is needed or when data coverage is limited. A hybrid strategy is therefore recommended: use empirical models to set conservative bounds and apply data-driven regressions to refine speed estimates where measurements exist. This combination improves reliability without sacrificing safety.

The work has certain limitations. The level-ice dataset had a narrow thickness range and few observations at the boundaries of operation. The ridged-ice dataset required preprocessing, and transient behavior is averaged out. As a result, the models describe quasi-steady speed but cannot predict actual transient loads and instantaneous speed, effectively providing minimum information about the risk of besetting. In the absence of information regarding the resistance from the consolidated layer or the level ice thickness part of a ridge, the h-v curve obtained through the empirical method is also not a standard to compare with; however, using the averaged ice thickness provides us an acceptable benchmark.

Future research should focus on improving the data and the modelling approach. First, synthetic data from numerical simulations can be used to strengthen the training dataset at operational limits. Second, dynamic machine-learning methods such as Recurrent Neural Networks (RNNs) or LSTMs (Long Short-Term Memory) could be introduced to model time-dependent interactions and capture inertia without manual lag correction or binning. Finally, hybrid physics-aware learning should be explored, blending resistance theory with data-driven prediction to ensure reliable behavior in both well-measured and sparse regions.

References

(SYKE), F. E. I. *Technical information of the research vessel Aranda*. Finnish Environment Institute (SYKE). Retrieved 17 Oct 2025 from https://itameri.fi/en/research-and-methods/research-vessel-aranda/tekniska-uppgifter/

Acanfora, M., Altosole, M., Balsamo, F., Micoli, L., & Campora, U. (2022). Simulation Modeling of a Ship Propulsion System in Waves for Control Purposes. *Journal of Marine Science and Engineering*, *10*(1), 36.

Caruso, D., Eudes, A., Sanfourche, M., Vissière, D., & Le Besnerais, G. (2017). A Robust Indoor/Outdoor Navigation Filter Fusing Data from Vision and Magneto-Inertial Measurement Unit. *Sensors*, *17*(12), 2795.

Enkvist, E. (1972). *On the ice resistance encountered by ships operation in the continuous mode of ice breaking* (24).

Erceg, S., & Ehlers, S. (2017). Semi-empirical level ice resistance prediction methods. *Ship Technology Research*, *64*(1), 1-14. https://doi.org/10.1080/09377255.2016.1277839

Fu, S., Zhang, D., Montewka, J., Yan, X., & Zio, E. (2016). Towards a probabilistic model for predicting ship besetting in ice in Arctic waters. *Reliability Engineering & System Safety*, *155*, 124-136. https://doi.org/10.1016/j.ress.2016.06.010

Gan, W., Ma, D., & Duan, Y. (2025). Comparisons of Machine Learning Methods in Ship Speed Prediction Based on Shipboard Observation. *Journal of Marine Science and Engineering*, *13*(6), 1011. https://doi.org/10.3390/jmse13061011

Geurts, P., Ernst, D., & Wehenkel, L. (2006). Extremely randomized trees. *Machine Learning*, *63*(1), 3-42. https://doi.org/10.1007/s10994-006-6226-1

Gong, H. (2023). *A review of numerical methods for estimating ship resistance in FSICR channel* (K544).

Haapala, J., Lönnroth, N., & Stössel, A. (2005). A numerical study of open water formation in sea ice. *Journal of Geophysical Research: Oceans*, *110*(C9). https://doi.org/https://doi.org/10.1029/2003JC002200

Huang, J., Diao, F., Ding, S., Han, S., Kujala, P., & Zhou, L. (2024). A Study on the Ice Resistance Characteristics of Ships in Rafted Ice Based on the Circumferential Crack Method. *Water*, *16*(6), 854.

Izumiyama, K. (2017). Ship Performance in Ice. In *Encyclopedia of Maritime and Offshore Engineering* (pp. 1-11). https://doi.org/https://doi.org/10.1002/9781118476406.emoe024

Jeong, S.-Y. (2024). Experimental investigation of ice load on a hull surface. *Journal of Advanced Marine Engineering and Technology*, *48*(6), 444-451. https://doi.org/10.5916/jamet.2024.48.6.444

Jeong, S.-Y. C., Kyungsik; Cho, Seong-Rak; Kang, Kuk-Jin; Lee, Chun-Ju. (2013). *A study of the resistance prediction method in level ice* 22nd International Conference on Port and Ocean Engineering under Arctic Conditions (POAC'13), Espoo, Finland.

Juva, M., & Riska, K. (2002). *ON THE POWER REQUIREMENT IN THE FINNISH-SWEDISH ICE CLASS RULES*.

Kaj, R. (2007). Design of Ice Breaking Ships. In *Encyclopedia of Life Support Systems (EOLSS)*. UNESCO – EOLSS.
Kuuliala, L., Kujala, P., Suominen, M., & Montewka, J. (2017). Estimating operability of ships in ridged ice fields. *Cold Regions Science and Technology*, *135*, 51-61. https://doi.org/10.1016/j.coldregions.2016.12.003
Lang, X., Wu, D., & Mao, W. (2024). Physics-informed machine learning models for ship speed prediction. *Expert Systems with Applications*, *238*, 121877. https://doi.org/10.1016/j.eswa.2023.121877
Li, F. (2016). *Evaluation of a Semi-Empirical Numerical Simulation Method for Level Ice Breaking* [Master's thesis (M.Sc. Tech.), Aalto University, School of Engineering]. Espoo, Finland. https://aaltodoc.aalto.fi/items/4248ec17-f1fa-41ca-b357-29e46bffc2d2
Li, F., Goerlandt, F., & Kujala, P. (2020). Numerical simulation of ship performance in level ice: A framework and a model. *Applied Ocean Research*, *102*, 102288. https://doi.org/https://doi.org/10.1016/j.apor.2020.102288
Li, F., Goerlandt, F., Kujala, P., Lehtiranta, J., & Lensu, M. (2018). Evaluation of selected state-of-the-art methods for ship transit simulation in various ice conditions based on full-scale measurement. *Cold Regions Science and Technology*, *151*, 94-108. https://doi.org/10.1016/j.coldregions.2018.03.008
Li, F., & Huang, L. (2022). A Review of Computational Simulation Methods for a Ship Advancing in Broken Ice. *Journal of Marine Science and Engineering*, *10*(2), 165.

Li, F., Montewka, J., Goerlandt, F., & Kujala, P. (2017, 2017/08//). A probabilistic model of ship performance in ice based on full-scale data. 2017 4th International Conference on Transportation Information and Safety (ICTIS),

Lindqvist, G. (1989, 1989). A straightforward method for calculation of ice resistance of ships. Proceedings of the 10th International Conference on Port and Ocean Engineering Under Arctic Conditions (POAC 1989),

Lindström, C. A. (1990). *Numerical simulation of ship manoeuvring motion in level ice* Proceedings of POLARTEC '90, Copenhagen, Denmark.

Lubbad, R., & Løset, S. (2011). A numerical model for real-time simulation of ship–ice interaction. *Cold Regions Science and Technology*, *65*(2), 111-127. https://doi.org/https://doi.org/10.1016/j.coldregions.2010.09.004

Malmberg, S. (1983). Omfartygs Fastkling i is (of Ship's Becoming Beset in Ice). *Helsinki University of Technology*.

Matala, R., & Suominen, M. (2022). Investigation of vessel resistance in model-scale brash ice channels and comparison to full-scale tests. *Cold Regions Science and Technology*, *201*, 103617. https://doi.org/10.1016/j.coldregions.2022.103617

Milaković, A.-S., Li, F., Marouf, M., & Ehlers, S. (2020). A machine learning-based method for simulation of ship speed profile in a complex ice field. *Ships and Offshore Structures*, *15*(9), 974-980. https://doi.org/10.1080/17445302.2019.1697075

Montewka, J., Goerlandt, F., Kujala, P., & Lensu, M. (2015). Towards probabilistic models for the prediction of a ship performance in dynamic ice.

Cold Regions Science and Technology, *112*, 14-28. https://doi.org/10.1016/j.coldregions.2014.12.009
Montewka, J., Goerlandt, F., Lensu, M., Kuuliala, L., & Guinness, R. (2019). Toward a hybrid model of ship performance in ice suitable for route planning purpose. *Proceedings of the Institution of Mechanical Engineers, Part O: Journal of Risk and Reliability*, *233*(1), 18-34. https://doi.org/10.1177/1748006x18764511
Norman, J. (1980). *Ice resistance prediction and motion simulation for ships operating in the continuous mode of icebreaking* [PhD thesis, The University of Michigan]. Ann Arbor, Michigan.
Rao, P. S., Kim, E., Smestad, B. B., Asbjørnslett, B. E., & Bhattacharyya, A. (2021). Predicting vessel speed in the Arctic without knowing ice conditions using AIS data and decision trees. *Maritime Transport Research*, *2*, 100024. https://doi.org/10.1016/j.martra.2021.100024
Riska, K., Wilhelmson, M., Englund, K., & Leiviskä, T. (1997). *Performance of merchant vessels in ice in the Baltic* (52).
S. A. Agulhas II. (2025). In *Wikipedia*: Wikimedia Foundation.
Sawamura, J., Riska, K., & Moan, T. (2008, 2008). Finite element analysis of fluid–ice interaction during ice bending. Proceedings of IAHR 2008,
Similä, M., & Lensu, M. (2018). Estimating the Speed of Ice-Going Ships by Integrating SAR Imagery and Ship Data from an Automatic Identification System. *Remote Sensing*, *10*(7), 1132. https://doi.org/10.3390/rs10071132
Su, B., Riska, K., & Moan, T. (2010). A numerical method for the prediction of ship performance in level ice. *Cold Regions Science and Technology*,

60(3), 177-188. https://doi.org/https://doi.org/10.1016/j.coldregions.2009.11.006

Suominen, M., Karhunen, J., Bekker, A., & Kujala, P. (2013, 2013/06/09/13). Full-Scale Measurements on Board PSRV S.A. Agulhas II in the Baltic Sea.*POAC Proceedings* POAC 2013 – 22nd International Conference on Port and Ocean Engineering under Arctic Conditions,

Suominen, M., Li, F., Lu, L., Kujala, P., Bekker, A., & Lehtiranta, J. (2020). Effect of Maneuvering on Ice-Induced Loading on Ship Hull: Dedicated Full-Scale Tests in the Baltic Sea. *Journal of Marine Science and Engineering*, *8*(10), 759. https://doi.org/10.3390/jmse8100759

SYKE, & FMI. (2016). *Aranda Cruise Report*.

Valanto, P., JONES, S. J., ENKVIST, E., & IZUMIYAMA, K. (2001). The resistance of ships in level ice. Discussion. Author's closure. *Transactions-Society of Naval Architects and Marine Engineers*, *109*, 53-83.

Weeks, W. F., & Hibler, W. D. (2010). *On sea ice*. University of Alaska Press.

Westerlund, A., & Lehtiranta, J. (2025). *BETTER SEA ICE FORECASTS FOR THE NORTHERN BALTIC SEA* (133).

World Meteorological Organization. (2014). *WMO Sea-Ice Nomenclature* (WMO-No. 259). https://library.wmo.int/viewer/41953/

Xie, C., Zhou, L., Wu, T., Liu, R., Zheng, S., Tsuprik, V. G., & Bekker, A. (2022). Resistance Performance of a Ship in Model-Scaled Brash Ice Fields Using CFD and DEM Coupling Model [Original Research]. *Frontiers in Energy Research*, *Volume 10 - 2022*. https://doi.org/10.3389/fenrg.2022.895948

Zhang, M., Sun, Q., Garme, K., Burman, M., & Zhou, L. (2022). Analysis of inland waterway ship performance in ice: Operation Time Window. *Ocean Engineering*, *263*, 112409. https://doi.org/10.1016/j.oceaneng.2022.112409

Zhao, P., Li, Y., & Zhang, Y. (2024). Ships are projected to navigate whole year-round along the North Sea route by 2100. *Communications Earth & Environment*, *5*(1), 407. https://doi.org/10.1038/s43247-024-01557-7